AN ABSTRACT OF THE THESIS OF

Robert Schriver for the degree of Master of Science in Sustainable Forest Management presented on September 6, 2018.

Title: Landscape Inventory and Harvest Strategies for Individual Western Juniper in Eastern Oregon

Abstract approved:

_____

Bogdan M Strimbu

Western juniper is a native species in eastern Oregon that became invasive during the last century since its range increased fivefold from 1936 to 1988. Western juniper's ability to absorb rainfall and groundwater has deleterious effects on stream flow and sensitive sage grouse habitat in eastern Oregon. New methods of western juniper remediation have been proposed, including harvesting and processing western juniper as merchantable timber. An essential part of these methods is the accurate survey of trees and a harvesting plan. The objective of my thesis was to estimate the existing juniper resource in Wheeler county, Oregon, and to develop a harvesting plan for the resource. To estimate the existing juniper resource, I implemented two methods of segmenting individual tree using their ground-projected crown and applied them to orthorectified multispectral aerial images. This work involved estimating the canopy height model from multispectral aerial imagery, which was performed with a generative adversarial network. The generated canopy height model was used with the most accurate tree crown detection method to create a map of juniper locations,

with their corresponding height. Based on the knowledge of location and size of each juniper I developed a novel individual tree level harvest strategy. The strategy was evaluated using two heuristic techniques, simulated annealing and record to record, on two areas, each of approximately 1600 ha. The results indicate that landscape restoration by removing junipers depends on the amount and value of the junipers, and in many cases, financial incentives would likely be needed.

Landscape Inventory and Harvest Strategies for Individual Western Juniper in Eastern Oregon

by
Robert Schriver

A THESIS

submitted to

Oregon State University

in partial fulfillment of
the requirements for the
degree of

Master of Science

Presented September 6, 2018
Commencement June 2019

Master of Science thesis of Robert Schriver presented on September 6, 2018

APPROVED:

Major Professor, representing Sustainable Forest Management

Head of the Department of Forest Engineering, Resources, and Management

Dean of the Graduate School

I understand that my thesis will become part of the permanent collection of Oregon State University libraries. My signature below authorizes release of my thesis to any reader upon request.

Robert Schriver, Author

ACKNOWLEDGEMENTS

The author expresses sincere appreciation for the help of Professor Bogdan Strimbu and Professor John Sessions for their guidance in creating this document. Thanks go to committee members Professor Fuxin Li and Professor Christopher Parrish of Oregon State University. Deserved thanks for Kendall Derby and all members of the *In The Sticks* Mill of Fossil, Oregon, and Herb Winters of the Wheeler County SWCD for their help collecting and milling western juniper for this project. This work was supported by the Forest Engineering, Resources and Management department at Oregon State University and the SUN Grant. Special thanks to my wife, Keavy, for her unending support.

TABLE OF CONTENTS

LIST OF FIGURES

Figure Page

LIST OF TABLES

1 Introduction

Western juniper is a native, invasive tree species in eastern Oregon. The extent of juniper savannahs, defined as having any amount of western juniper canopy cover, has increased more than five times since 1938 (Miller and Rose, 1995). Furthermore, the extent of forests with more than 10% western juniper reached over 1.3 million acres (Azuma *et al.*, 2005), which is six times more than the estimated juniper in 1938 (Miller, 2005). Growing in a high elevation steppe of the intermountain west, western juniper has adapted to have a large root area relative to its size (Jeppesen, 1977), which is capable of absorbing significant amount of groundwater. Therefore, western juniper remediation is a priority for watershed managers throughout eastern Oregon, to increasing range productivity and stream flows (Gedney *et al.*, 1999), as well as to recover the habitat of endangered species, like the sage grouse (Baruch-Mordo *et al.*, 2013). Current juniper remediation techniques focus on removing the trees onsite, either by felling or burning (Miller, 2005). The low density and reduced economic value of the vast majority of junipers, concentrates the remediation to sensitive habitats. Processing juniper to create marketable wood products has been proposed as a remediation technique that might make more habitat restoration possible, since the value of processed juniper could be used to offset the cost of removal. However, processing juniper requires prior knowledge of the value of juniper, to estimate the potential profit from harvesting. The combination of a sparse presence on the landscape with the low economic value make infeasible conventional forest inventory methods, which rely on sampling (Nielsen *et al.*, 2013). Therefore, in this work, I describe two methods of estimating

juniper location and height from remotely sensed imagery, which makes surveying juniper over large areas feasible. Accurate information on the location and amount of juniper allows estimation of the value of junipers. Consequently, in this work I investigate two methods of creating a tree harvest schedule that uses as elementary harvest unit individual juniper. In concert, these methods can be used to detect, estimate value, and develop a harvest plan for western juniper in eastern Oregon.

1.1 Thesis organization

The thesis contains four chapters, structured as followed:

Chapter 1. Introduction. In the introductory chapter I will describe the problem and lay out the structure of the thesis.

Chapter 2. Generative adversarial networks for tree crown extraction and measurement. In the second chapter of the thesis I will apply two methods based on deep convolutional neural networks to the problem of tree crown detection. I also apply a generative adversarial network to the problem of individual tree height measurement.

Chapter 3. Optimal tree level strategies for harvesting western juniper. The third chapter presents two strategies of harvesting junipers at the individual tree level

Chapter 4. Conclusion. In the final chapter of my thesis I will summarize the finding of the previous two chapters.

2 Deep convolutional neural networks for tree crown detection and measurement

2.1 Introduction

Traditional forestry techniques can require extensive field measurement to estimate many parameters relevant to forest management, such as tree density, total height, or diameter at breast height. A large field effort is often infeasible due to the size of the forest or the costs involved in manual collection. Furthermore, in sparse and irregular stands, such as those found within the juniper savannah in Oregon, the effectiveness of manual forest measurement is reduced. For large forestry projects remotely sensed data are used in estimation of the parameters of interest (Nielsen *et al.*, 2013). There is a long history showing that remotely sensed imagery can lead to accurate forest inventory, even at tree level, particularly for tree cover (Hulet *et al.*, 2014) and tree height (Næsset, 2002). The ability of remote sensing to provide fast and inexpensive estimates is particularly attractive for forest inventories exhibiting difficult conditions, such as the sparse juniper woodland (Nielsen *et al.*, 2013). Inventory of dispersed trees is expensive because large areas have to be cruised if traditional forest estimation techniques are used. However, obtaining tree metrics at the landscape scale has been made possible over the past decades because of the proliferation of high resolution remotely sensed data. A large array of methods are available for forest inventory from remote sensed data (Zhen *et al.*, 2016), most of them focused on tree count and total height. Depending on data format and the approach used to estimate forest attributes, the methods can be separated in two categories: raster-based and vector-based. Raster based methods use as input two-dimensional data of fixed scale,

typically imagery, whereas vector based methods uses as input unstructured three dimensional data, like lidar. Because raster-based estimates are obtained using a predefined grid, the results depend on the scale. The dimension of the grid, which is selected according to the type of and size of the forest, plays a significant role in the quality of the results. Vector based estimates are scale free, but collecting and processing unstructured three dimensional data can be costly and difficult.
Forest inventory methods can be also separated according to the perspective of the device recording the data from which the attributes will be estimated. From this perspective, there are nadir view methods, which use data describing the upper part of the forest, and side or zenith view methods, which use data describing the lower part of the forest. The first step to estimate attributes of individual trees from nadir acquired data is to segment the crown of each tree, then compute the values of interests, such as total height or height to the base of live crown. When side or zenith acquired data are used in estimation, then the focus is on segmenting individual stems, followed by diameters along the trunk.

Most forest inventories identify species, the number of trees, and the size of the trees (Avery and Burkhart, 2015; Kershaw *et al.*, 2017). One of the most common strategies in tree identification is segmentation of crowns (Chen *et al.*, 2006; Jakubowski *et al.*, 2013; Camps-Valls *et al.*, 2014; Ayrey *et al.*, 2017). Individual tree crown detection methods can be roughly separated between those which operate on 2D data, like nadir or near nadir imagery, and those which operate on 3D data, like lidar or photogrammetric point clouds (Zhen *et al.*, 2016). Jakubowski *et al.* (2013)

found that tree crown detectors applied to three-dimensional data outperformed those applied to two-dimensional data. Arguably, the most popular methods used to delineate individual tree crowns are feature based algorithms (Camps-Valls *et al.*, 2014; Long *et al.*, 2015; Strimbu and Strimbu, 2015; Ayrey *et al.*, 2017). Feature based methods use properties describing the forest to distinguish trees crowns from neighboring entities, such as vegetation or adjacent tree crowns, within a remotely sensed scene. Watershed segmentation (WS) (Wang *et al.*, 2004) and spatial wavelet analysis (SWA) (Strand *et al.*, 2006) are two commonly encountered procedures from this broadly defined class of algorithms (Kaartinen *et al.*, 2012). Conceptually, in WS, tree crowns are represented as revered watersheds. Individual crowns are detected starting from local canopy maxima, representing a possible top of a tree crown, which is used as a fill point or sink for the inverted tree crown. Subsequent to the identification of the sink points, crowns are delineated similarly to basins from watershed analysis. SWA exploits both local maxima and the relative circular shape of tree crowns, as seen from nadir. A wavelet, like the Mexican hat function is convolved along the image at different scales. This wavelet is shaped to be at a maximum value when it is convolved on an object with an identical, or near identical radius, and a local maxima at its center, which roughly describes a tree in nadir imagery. Poznanovic *et al.* (2014) found that SWA performed favorably when compared to other feature-based method for individual juniper detection in southeastern Oregon. Both of these feature-based methods work similarly on both spectral and lidar data, since the tallest point of an object, in the trees case the treetop, is a local maxima in terms of spectral value in a nadir image (Wang *et al.*, 2004).

Object based image analysis allows a user to define feature-based rules for tree crown detection, and, as the name suggests, focuses on the full object to be detected, which differs from a pixel by pixel approach (Blaschke, 2010). Hulet *et al.* (2014) explored the used of the object based image analysis for the purpose of juniper tree crown detection for canopy cover estimation. Skurikhin *et al.* (2013) found that individual tree crown detection methods can work well for sparse canopies (<20% canopy cover), which characterizes landscapes dominated by juniper.

Another class of individual tree crown detectors are based on the concept of machine learning (Bengio *et al.*, 2013; Längkvist *et al.*, 2016), which uses training data to create a model for tree crown location and sizes. Although these methods have a costly ground-truth generation step, a learned model can find features that may have been missed by other methods; therefore, have a superior predictability (Zhen *et al.*, 2016). Deep convolutional neural networks (CNN), which are a class of machine learning model, have recently been applied to tree identification (Längkvist *et al.*, 2016). Li *et al.* (2016) implemented a sliding window CNN for detection of individual trees from satellite imagery in palm plantations. Wegner *et al.* (2016) used Faster Region-based CNN (Faster RCNN), which is an object detection model based on deep CNNs, to catalog urban trees using remotely sensed imagery.

Multidimensional data can increase the accuracy of individual tree crown detection (Jakubowski *et al.*, 2013). Jakubowski *et al.* (2013) compared the accuracy of individual tree crown detection methods on both 2D data, from aerial imagery, and

3D data, derived from photogrammetry, and found that three-dimensional data outperformed the object based image analysis segmentation technique. However, in many areas there are no 3D data available, which means that algorithms which require 3D inputs cannot be directly applied. Previous work has explored estimating 3D data from 2D imagery, and found that texture metrics were important predictors for juniper stand metrics, such as average tree height and volume (Nielsen *et al.*, 2013). In their study, the texture metrics were derived from scattered lidar collections and modeled using random forests. Recently, the focus has shifted towards 3D estimation with the potentially more powerful predictive modeling of deep CNNs. Rather than predicting a full point cloud, Ghamisi and Yokoya (2018) describe the use of a generative adversarial network (GAN) to generate a rasterized digital surface model from satellite imagery. GANs are a class of deep neural networks that are commonly used for image generation, and have been shown to be powerful models for the generalized problem of paired image to image translation (Isola *et al.*, 2017), where a target image is predicted from an available image source.

In eastern Oregon, juniper presents considerable variation in projected crown and canopy cover (Gedney *et al.*, 1999). For sparse canopies, individual tree crown detection has been shown to perform well for extracting canopy metrics (Skurikhin *et al.*, 2013). For this reason, we chose to investigate the use of two individual tree crown detection techniques to extract metrics for western juniper at the landscape scale. These methods are based on Faster R-CNN (Ren *et al.*, 2015) and a watershed

detection algorithm augmented by a canopy height model (CHM) generated from a GAN.

Depending on the objective, management of western juniper is based on individual trees or on trees aggregated to a fixed scale. For example, juniper stand age and canopy cover are important in determining priority areas for restoring sage-grouse habitat (Baruch-Mordo *et al.*, 2013). Nielsen *et al.* (2013) created a model based on spectral data to predict aggregated metrics at a 30-meter scale for western juniper and found it more accurate than performing individual tree crown detection and aggregating the detected crowns. The aggregated metrics included a texture component, which was modeled from lidar data adjacent to their study area. The texture proved vital to the accuracy, demonstrating the usefulness of 3D data for predicting canopy statistics. The individual tree crown detection methods used for comparison were based only on spectral data and did not include a texture model. Furthermore, availability of tree level information, even relatively erroneous, adds a spatial dimension to the data that is not available to aggregated data, and which also allows for operations on a variety of different scales, as opposed to the fixed scale of aggregated data. Therefore, the objective of this study is to estimate the location and size of western junipers within Wheeler County, Oregon. To achieve this task we focused on individual tree crown detection enhanced by a 3D surface model, which will be used to estimate the size of detected tree crowns.

2.2 Methods

2.2.1 Study Area

The study was triggered by the North Slope Ochoco Holistic Restoration Project, which was funded by the USA Natural Resources Conservation Service. The project area is defined by the watershed of three tributaries of the John Day River, namely Cherry, Bridge, and Mountain Creeks (Figure 1). The study area is comprised mostly of rangeland, and sparse juniper woodlands, but a significant percentage in the southern portion of the study area contains denser forests, comprised of a mix of ponderosa pine and western juniper. The main challenge when considering detecting, measuring, and planning harvests of individual trees in this study area is size, since the site comprises approximately 350,000 acres.

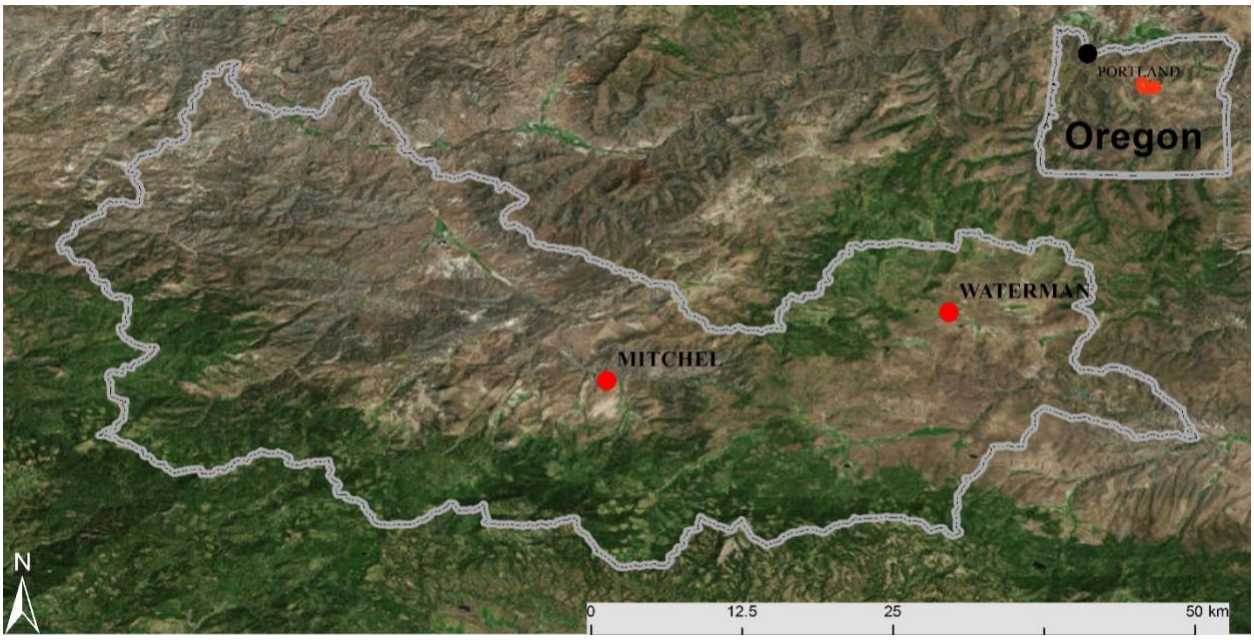

Figure 1. Study area overlaid on the NAIP imagery

2.2.2 Remotely Sensed Data

2.2.2.1 Input Data

The images used in this study were collected for the National Aerial Imagery Program (NAIP) in 2009. This collection is freely available, and is of a higher spatial resolution than later imagery collections. The images have four bands, red, green blue, and near infrared, and a spatial resolution of 0.5 m, making them suitable for vegetation monitoring and detection (Ke and Quackenbush, 2011). We chose to use the red (R) and near infrared (NIR) bands, after determining that use of the blue (B) and green (G) bands did not provide any significant benefit to our analysis.

(Davies *et al.*, 2010) suggested that environmental factors, specifically elevation and aspect, are key indicators of potential juniper cover. Therefore, in addition to spectral data, we also used for delineation of tree canopy a hillshade raster derived from the 10-meter DTM from the USGS (Archuleta *et al.*, 2017). The hillshade provides aspect and spatial relationship to neighboring raster cells to our predictive models.

Lidar derived data products, such as digital elevation models, are provided by the Oregon Department of Geology for many locations within Oregon. For our study we used the Pine Creek collection performed in 2011 and the Ochoco West collection performed in 2013, which intersect our study area. For the Pine Creek dataset, we used the full extent of collected data, which includes data collected outside our study area. This data was chosen since the forest canopy structure across the Pine Creek area closely matched the forest structure within our study area. The majority of the Ochoco West lidar covered dense ponderosa pine forests, which make up only a small portion of our study area. For this reason, we only use data from the Ochoco West dataset which lies within our study area, to match the forest structure types within the

Cherry, Bridge, and Mountain Creek watersheds. We used two digital elevation models in the study, one describing the terrain (DTM) and one describing the surface (DSM), both with 1-meter resolution. The canopy height model (CHM) can be obtained by simply subtracting the DTM from the DSM. Each pixel in a CHM represents the relative height above the ground. Since a CHM provides a 3D structure of a canopy, it is often used for individual tree crown detection (Zhen *et al.*, 2016).

2.2.2.2 Data Preprocessing

The predictive modelling techniques we explore are designed to be used with 3-band imagery with 8 bits per pixel. Using a trial and error approach, we found that the bands with the most predictive power for vegetation detection were red (R) and near infrared (NIR) bands, which are also commonly used in many vegetation health indices (Bannari *et al.*, 1995). In addition to differentiating between vegetation and non-vegetation, the R and NIR bands are also useful for separating vegetation from unhealthy or dead vegetation, which are not the focus of the study. Environmental data, such as rainfall and terrain have also been shown to explain some tree structure characteristics of western juniper (Davies *et al.*, 2010). Our intuition in including environmental data was that forest structure prediction would create a more accurate canopy height model. Since we were restricted to only three bands, we chose to incorporate hillshade data as the last band in our image. The hillshade raster provides a consistent representation of aspect, as well as some spatial terrain data. For example, a convolutional filter applied to a hillshade raster could potentially determine which points were in canyons by detecting sharp changes in hillshade, as shown in (Figure 2). To combine the 10-meter resolution hillshade with our 0.5-meter

resolution imagery, we resampled the hillshade data using a nearest neighbor technique.

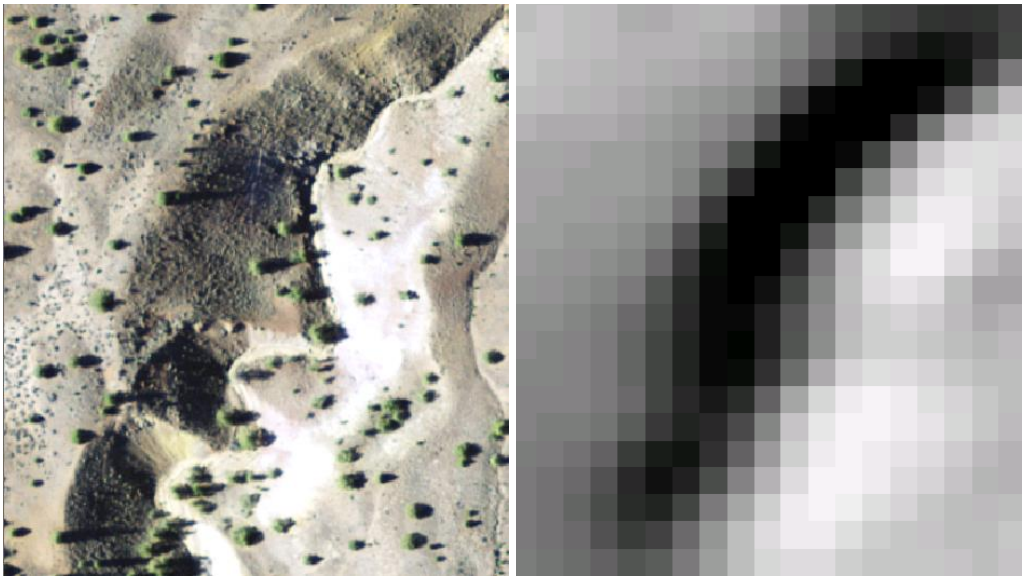

Figure 2. Example hillshade raster showing complex terrain

We combined the three bands in a raster that contains red in the first band, near infrared in the second band, and hillshade in the third band. An example of the false color image with the three bands is shown in Figure 3.

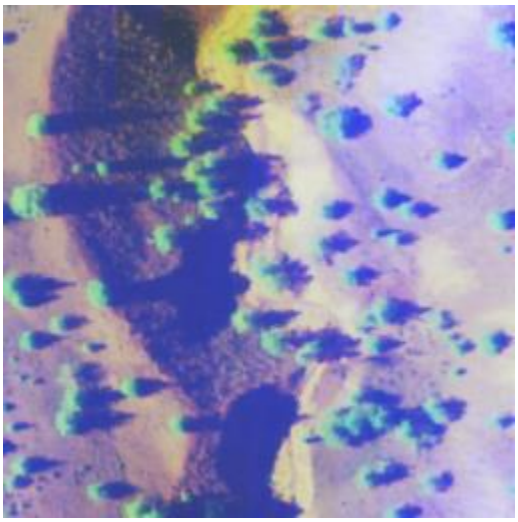

Figure 3. A false color red, near infrared, and hillshade portion of an image

Imagery collected of objects with a sufficiently large angle between the sensor and object can lead to situations where a tall object, like a tree, appears ‘tilted’, and is commonly referred to as relief displacement (Figure 4). Lidar data on the other hand, by recording the location of each return, is minimally affected by departure from nadir. The tilt of the objects away from the principal points (Lillesand et al) can lead to misalignment between lidar derived data, like our CHM, and aerial imagery. Based on the work of (Safdarinezhad *et al.*, 2017), we perform an alignment routine based on the hypothesis that for our imagery and digital surface model, which is dominated by vegetation, overlap between pixels containing elevations above ground and vegetation should be greatest when the images are correctly aligned. Alignment determined in this manner was consistent across NAIP and lidar derived images.

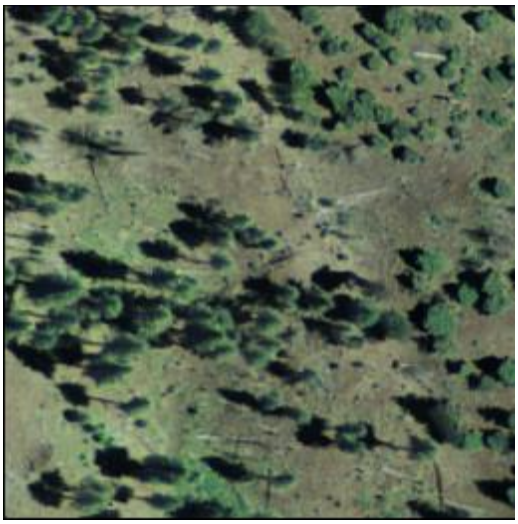

Figure 4. Effect of non-nadir viewpoint on image object location

2.2.3 Tree Crown Identification

2.2.3.1 Faster RCNN

Convolutional object detectors have seen great success in general object detection (Ren *et al.*, 2015), as well as success in object detection in remote sensing (Tang *et al.*, 2017). For our study, we used the Faster RCNN implementation in the Tensorflow Object Detection Framework (Huang *et al.*, 2017). This framework allowed for rapid and consistent configuration, as well as potential extension in the future to newly develop object detection models. The basic unit in most object detection models is a bounding box that contains the objects to be identified.

Trained operators created ground truth tree location data by visually interpreting the NAIP imagery. The images within the study area were split into 50 by 50 meter chips, to allow for a random sample of locations within each image to be drawn. For each observed tree crown which was at least 50 percent within a chip, a corresponding bounding box was created. Bounding boxes below 9 square meters were removed, as the crown area of these detections likely corresponds to a juniper tree height less than 1.8 m, which is below the threshold selected for delineating woody vegetation from non-woody vegetation. Bounding boxes were digitized using labelImg (Tzutalin, 2015). Overall, 750 chips were processed, with a total of 8111 individual tree detections. Chips were chosen to obtain a representative sample of canopy cover percentages and tree species that exist within the chip sample area.

The ground truth boxes were randomly split 70/30 into training and testing datasets,

similar to (Li *et al.*, 2016).To increase the effective number of training images we augmented the dataset, which has been shown to reduce overfitting and improve performance for small datasets (Ronneberger *et al.*, 2015). In general, data collected at a nadir viewpoint is rotation invariant (Cheng *et al.*, 2016), which means we can rotate the image up to 270 degrees, and flip along any axis, and the resulting image will still be a valid representation of the ground truth data. In addition to data augmentation through rotation, we configured the Tensorflow Object Detection framework to randomly crop and pad images to their original size. This ensured that the resulting cropped images would have objects of the same scale as non-cropped images. These data augmentations allowed us to extend our small dataset enough to avoid overfitting.

Appropriate anchor box sizes and aspect ratios are two of the most important parameters for accurate detection with Faster RCNN, especially when detecting small objects (Eggert *et al.*, 2017). Anchor boxes are used by Faster RCNN as the basic unit of object detection. At a fixed grid of points, the model estimates the likelihood that an object exists within that anchor box, centered at that point. Each anchor box in the Tensorflow Object Detection framework is defined as a square box size, and a set of aspect ratios. These aspect ratios can be used to capture rectangular objects. Anchor box sizes, and aspect ratios, should be chosen to fit the set of object sizes in the dataset (Eggert *et al.*, 2017). The main tradeoff between adding a new anchor box is speed, so a small, but representative set of anchor boxes must be chosen. To determine the set of boxes and aspect ratios appropriate for our dataset we first chose a number of anchor boxes (i.e., six) and aspect ratios (i.e., three) that would provide

an acceptable range and running time. Second, we performed a histogram analysis of bounding box side length, choosing to split the histogram in six bins, as recommended by (Eggert *et al.*, 2017). We performed a similar analysis on the histogram of bounding box aspect ratios, and found that almost all tree crowns are roughly square, and fit within the base aspect ratio of 1.0. In order to capture those crowns which deviated slightly from this ratio, we also configured the framework to amend the chosen base anchor box sizes with aspect ratios of 0.75 and 1.25.

Table 1. Anchor box sizes for Faster RCNN

Box Number	Box Size		
	As a ratio of base size (256x256)	In square pixels	In GSD (square meters)
1	0.10375	28	7
2	0.140625	36	9
3	0.171875	44	11
4	0.203125	52	13
5	0.25	64	16
6	0.5	128	32

2.2.3.2 Generative Adversarial Network

We used a GAN to generate an estimated canopy height model for areas within our study site that do not have available lidar data. The input for the GAN is the multispectral NAIP images, which are available for the entire study area. This transformation belongs to a class of problems known as the paired image to image translation problem, which GANs are particularly well suited for (Isola *et al.*, 2017).

We use the pix2pix framework which was developed for the paired image to image translation problem (Isola *et al.,* 2017). Training and testing data was generated by splitting the input data (i.e., Red, NIR, and hillshade), the ground truth data, and the canopy height model into paired chips, each 256 x 256 pixels. For the Pine Creek and Ochoco West, clipped to the extent of the lidar data, we obtained approximately 50,000 image pairs, which we split 70/30 between training and evaluation. The majority of the CHM values are zero or near zero. Therefore, we used a modified L1 loss function (Equation 1) to properly weight the class of pixel we are generating (Long *et al.,* 2015). The modified L1 loss is defined by a threshold, in our case 1.8 m. The threshold was chosen based on field measurements of western juniper height and represents the minimum crown height of potentially harvestable trees. The threshold is also supported by the distribution of heights (Figure 5), as a peak starts around 6 ft. The vast majority of non-zero elevation values represents woody vegetation, so we use the threshold as a separator of ground from woody vegetation.

$$Modified\ L1\ Loss = \begin{cases} 0 & if\ y_{true} < 6 \\ abs(y_{true} - y_{predicted}) & if\ y_{true} \geq 6 \end{cases}$$

Equation 1: Modified L1 loss

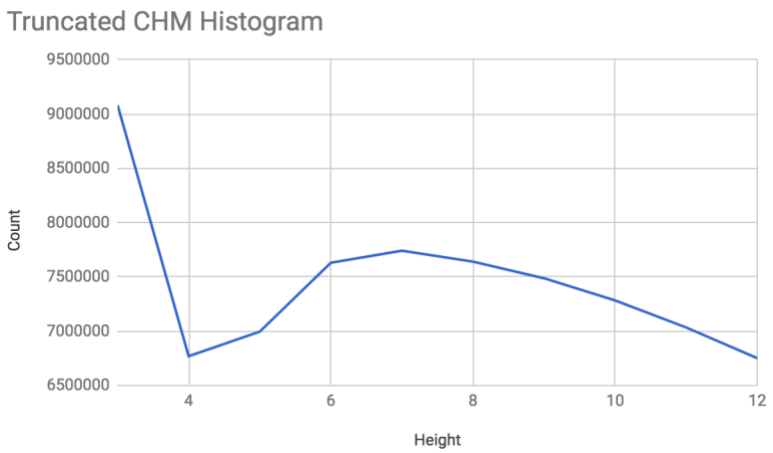

Figure 5. Truncated CHM histogram

2.2.3.3 Multi-scale Watershed Detection

We apply a multi-scale watershed segmentation technique, adapted from Wang *et al.* (2004), on both the generated three-dimensional data and two-dimensional imagery, and compared results to photo-interpreted ground truth. Our method of individual tree crown detection is based off the work of Wang *et al.* (2004), where a multi-scale local maxima filter is used to determine tree local maxima, followed by a watershed segmentation to segment individual tree crowns. We modify the method of Wang *et al.* (2004) slightly, since our study area contains large areas of non-woody vegetation and some human created structures, which must be filtered before local maxima detection.

To match the format of input data in (Wang *et al.*, 2004), we perform two main preprocessing steps. First, we create a mask of vegetation, using a threshold. We base this threshold off the NDVI, which is the normalized difference between the red and infrared spectral data. Using NDVI also gives us the benefit of filtering out some non-living juniper, since unhealthy vegetation is also filtered when setting this threshold.

We set this threshold at 0.6 for our study, which was determined by trial and error and assessing the precision and accuracy metrics after iterating through a set of potential NDVI thresholds. Second, we create a mask of height, using a threshold on the generated CHM. This mask is used to differentiate woody and non-woody vegetation. The threshold we chose was 6 feet, based on Figure 5. Since the non-ground pixels in our CHM are dominated by woody vegetation, we interpret the dip in Figure 5 as the separation between ground and noise CHM pixels, and non-ground, woody vegetation.

We then perform a dilation of 1 pixel on both masks, individually, to close any gaps in the mask, since we expect neighboring pixels to belong to the same class (i.e., a pixel next to, or surrounded by pixels labeled as vegetation, is likely also vegetation). Intersecting the masks provides the location of the woody vegetation. The intersection filters the generated CHM by removing the non-woody vegetation, in preparation for further image processing. Based on the work of Wang *et al.* (2004), we perform a multi-scale maxima filter on our generated CHM. The purpose of this filter is to smooth within crown local maxima, which could be caused by tree branches or noise within our CHM generation. For our study, we used a circular maxima filter with radii of 1, 2, and 3 meters. These radii were chosen from field observation of western juniper, as well as an analysis of the distribution of juniper crown sizes from photo interpretation of aerial imagery. A circular filter was chosen to match the roughly circular shape of western juniper crowns in the CHM. For each scale, we then computed a flow direction map. This mapping transforms an elevation raster, in our case a CHM, into a raster with each pixel storing the direction of the water ‘flow’ if it

would be placed at that elevation. This transformation is an intermediate step in traditional watershed segmentation (Ke and Quackenbush, 2011). Pixels with a zero flow value represent our local elevation maxima, which should correspond to the tops of trees. Due to the maxima filtering applied beforehand, this treetop is blurred into a set of pixels, with the estimated treetop lying in the middle of the set of pixels. One of the major problems in tree crown detection is differentiating within crown local maxima, and canopy height local maxima (Wang *et al.*, 2004). The purpose of this multi-scale approach is that canopy height local maxima are maxima at all, or most scales of maxima filtering, whereas within crown maxima are only local maxima in a minority of the chosen scales. The three flow maps, corresponding to the different maxima scales, are combined together using a majority filter on corresponding pixels, ensuring that only those pixels which are maxima at multiple scales are preserved. Our method of determining tree crown location from multiple scales of watershed can also be applied to just multispectral imagery. To determine the difference in accuracy between crown segmentation based only on imagery and on the enhancement of imagery with a generated CHM, we performed the multi-scale watershed segmentation using only NAIP imagery. Since we no longer have a CHM to aid in filtering below a certain height, we base our initial segmentation only on NDVI indices. The raster used for maxima filtering is also changed from the generated CHM to the NDVI raster.

2.2.4 Tree Crown Measurement

Beyond detection, deriving tree crown metrics can provide additional useful information for tree harvest and forest management. Using both two and three-

dimensional data, crown shape and area can be determined from watershed segmentation (Zhen *et al.*, 2016). We use the detected treetop as a sink, or flow output, and treat our local maxima filter raster as an elevation map. From there, we can use a watershed delineation algorithm, like Wang *et al.* (2004), to determine the extent of each individual tree crown within each tree cluster. This method has been applied by Poznanovic *et al.* (2014) to estimate juniper crown area using spectral imagery.

The generated CHM provides us with 3D data, which allows identification of the crown shape, and tree height. Tree height is of particular interest, since it is a predictor of western juniper volume, which can be used to estimate merchantable value. We estimate the tree height as the maximum value of the CHM within the estimated tree crown.

2.3 Results

2.3.1 Generative Adversarial Network

Evaluation of GAN is challenging, as depends on the problem, particularly for the image generation problem. Metrics typically either attempt to evaluate the qualitative value of the generated images or perform a quantitative analysis of the generated distribution in comparison to the ground truth, or 'real world' distribution of images (Zhu *et al.*, 2017). Qualitative measurements rely on extensive manual image analysis, which is infeasible for this study. Since generated pixels correspond to a real-world height measurement, as opposed to other image generation tasks, where the pixel values do not have an obvious physical meaning, we used a quantitative assessment of GAN performance. Because the GAN produced a CHM, which can be

converted to heights, the main tool we use for GAN assessment is the histogram of heights. We have developed two histograms, each with 0.3 m bins: one for lidar based CHM and one for GAN generated CHM. The difference between the ground truth height histogram and the generated CHM histogram is an aggregate measure of accuracy of the estimated individual tree height. We assessed the departure between the two histograms using the two-sample Kolmogorov-Smirnov (KS) tests.

The volume and height of western juniper are positively correlated [Dodson]. Therefore, an underestimation of tree height would lead to an underestimation of tree value. Harvesting and processing larger trees is more efficient from an economic perspective, due to the large time-labor cost associated with changing logs on a manual mill typically used for western juniper processing. Since we are also only concerned with height measurements for woody vegetation, which we classify to be taller than 1.8 m, we only assessed the divergence of height distribution above 1.8 m. Since we use CHM derived from two separate lidar datasets, we wished to compare GANs trained on a combined dataset, as well as on individual lidar datasets. KS test revealed that there is no difference ($p>0.9$) between the histograms of the CHM produced from lidar and from GAN (Table 2). Additionally, we explored the effect of different loss functions, including the default L1 loss for pix2pix (Isola *et al.*, 2017), as well as removing the adversarial loss component. The KS test supplied the same conclusion that the lidar and generated height histograms are not different (Table 3).

Table 2. Kolmogorov-Smirnov distance for generated and ground truth histograms of models trained on separate datasets. All values are not significant, as p-values > 0.9

Histogram\Model	Modified L1 Loss +	Modified L1 Loss +	Modified L1 Loss +

	Wheeler Ochoco + Pine Creek	Wheeler Ochoco	Pine Creek
Wheeler Ococo + Pine Creek	**0.011**	0.022	0.037
Pine Creek	0.003	0.025	**0.001**
Wheeler Ochoco	0.026	**0.01**	0.107

Table 3. Kolmogorov-Smirnov distance for model histograms trained with different loss functions

Distribution\Model	Modified L1 Loss + Wheeler Ochoco + Pine Creek	L1 Loss + Wheeler Ochoco + Pine Creek	L1 Loss + No Adversarial Loss + Wheeler Ochoco + Pine Creek
Wheeler Ococo + Pine Creek	**0.011**	0.023	0.016
Pine Creek	**0.003**	0.020	0.027
Wheeler Ochoco	**0.026**	0.027	0.038

Pixel-wise RMSE was considered as an additional metric for GAN selection. We hypothesized that a network with a lower pixel-wise RMSE value would estimate individual tree heights with more accuracy. The results for pixel-wise RMSE calculated between the ground truth dataset and the generated datasets suggests that the GAN with an L1 Loss function, no adversarial loss, and trained on both areas performs the best using the RMSE metric (Table 4).

Table 4. Pixel-wise RMSE of generated CHM

Distribution\ Model	Modified L1 Loss + Wheeler Ochoco + Pine Creek	Modified L1 Loss + Wheeler Ochoco	Modified L1 Loss + Pine Creek	L1 Loss + Wheeler Ochoco + Pine Creek	L1 Loss + No Adversarial Loss + Wheeler Ochoco + Pine Creek

Wheeler Ococo + Pine Creek	18.782	19.279	19.031	16.36	**13.135**
Pine Creek	5.856	5.768	10.176	5.816	**4.275**
Wheeler Ochoco	28.346	31.699	29.291	26.121	**19.338**

2.3.2 Tree Crown Detection

Ground truth tree crowns were digitized from the 2009 NAIP dataset, which was also used as our predictive spectral data for all tree crown detection methods we evaluated. We use the same bounding boxes to both evaluate the Faster RCNN network and tree crown detection methods. For Faster RCNN, detections were determined at 0.5 confidence, and were counted as a true positive if the intersection over union (IoU) was greater than 0.1.

Each estimated treetop was converted into a point detection by taking the centroid of the detected polygon. Since some ground truth polygons were of trees which were only partially within the grid cell, it is possible that a detected tree point could correspond to a ground truth polygon but lie outside of it. For this reason, we allowed for detected tree points to lie within a buffer of a ground truth polygon and still count as a true positive. For our study area, this buffer was set to two meters. Each tree point was assigned to its spatially closest bounding box. If multiple detected tree points were assigned to a single ground truth, only the closest point was counted as a true positive, and all other points were counted as a false positive. The metrics used for assessment are mean of precision (Eq. 2), recall (Eq. 3), and the F1 score (Eq. 4).

$$precision = \frac{true\ positive}{true\ positive + false\ positve} \quad 2$$

$$recall = \frac{true\ positive}{true\ positive + false\ negative} \quad 3$$

$$f1 = 2 * \frac{precision * recall}{precision + recall} \quad 4$$

Table 5. Individual tree detection metrics. MSWD stands for multiscale watershed detection

Algorithm	Assessment metric				
	Recall	Precision	F1	Omission error	Commission error
2D MSWD	0.813	0.533	0.644	0.713	0.187
3D MSWD	0.706	0.761	0.733	0.222	0.294
Faster RCNN	0.735	0.913	0.814	0.070	0.265

2.3.3 Aggregated Tree Statistics

Since our method can also produce aggregated statistics, we compare our results from aggregation to work by (Nielsen *et al.,* 2013). Ground truth for this comparison was taken from our digitized tree crown polygons. Since our polygons were digitized using 50-meter grid cell size, and at a different grid offset, we converted the digitized polygons into estimated canopy cover at a 30-meter grid cell size, for which we use a method adopted from (Nielsen *et al.*, 2014). If the ground truth chip outline, representing the image basis for digitization, contains at least 50% of the grid cell, we assume that the canopy cover estimated for that grid cell from polygon area is accurate. We then normalize the total canopy cover from digitized polygons by the amount of overlapping area between the chip and ground cell to get an estimate of canopy cover percentage. We computed the difference from ground truth between our individual tree crown detection method and the random forest work of (Nielsen *et al.*, 2013) by averaging the absolute value of the difference between the ground truth and estimated canopy cover. The results reveled that our method is superior to

random forests, by almost 50%, as it produced an absolute error of 4.98% compared with random forests (Nielsen *et al.,* 2013) that had 8.63%.

2.4 Discussion

2.4.1 Generative Adversarial Network

Training the GAN to produce a high-quality CHM was challenged by the fact that our ground truth data came from two different data sources, collected in two different years, and at a different time of year. Since a forest is a system that is constantly changing, the discrepancies in data could lead to inconsistent learning from the network, especially considering that lidar collections from different years may have different height distributions, not necessarily explained by the dynamics of the juniper ecosystem. We found that using only one dataset for training led to a network which did not fit the natural distribution of heights from the CHM. To determine the effect of the addition of lidar from different years, we compare networks trained on only the Pine Creek lidar dataset, Ochoco West lidar dataset, and the combination of both datasets (Table 2). We can see that the height histogram generated from each network most closely matches the height histogram of the data used to train the network. However, the network trained from the combined dataset was able to closely match each datasets height histogram, as well as the combined dataset height histogram. Our

results confirm the findings of (Hulet *et al.*, 2014), where datasets collected from different years were not found to be significantly different.

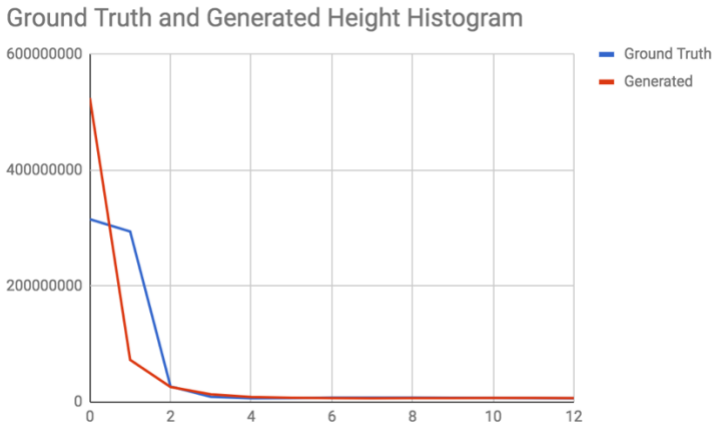

Figure 6. Truncated histogram for ground truth and generated heights

The Ochoco West project area is dominated by dense ponderosa pine stands, whereas the Pine Creek project area is defined by low density juniper savannah. The large difference in RSME is likely due to the larger heights of ponderosa pine, where the height difference between trees and ground are much larger. Any misestimation by the generator network is therefore highlighted due to the outlier magnification of RMSE. Unsuitability of RMSE for estimating the network performance can be inferred from the observation that the worst method, as described by KS test, was the best when considering RMSE.

2.4.2 Faster RCNN

2.4.2.1 Tree Classification

One of the potential benefits of a convolutional object detector which we explored was the ability to classify as well as to detect tree crowns. Classifying trees from

remotely sensed imagery has been explored by (Wegner *et al.*, 2016), and Faster RCNN has been used to both detect and classify between coniferous and broadleaf trees. The two major tree species in our study area which we would like to classify are western juniper and ponderosa pine, both coniferous species. However, the framework we chose is designed to work with 8-bit, three band images. This restriction precluded the inclusion in the network of environmental variables, like elevation, which can range from 1400 to 6800 feet within our study area. Future work could explore working with a different convolutional object detection framework, which could allow for data that cannot be represented in a 24bpp format. We found that this restriction prevented accurate classification between western juniper and ponderosa pine. For this reason, we modified our dataset to contain a single class of type 'tree', which aligned Faster RCNN with other tree detection algorithms focused only on detection rather than classification.

2.4.2.2 Small Object Detection

Tree detection in remote sensing is a combination of some of the worst-case scenarios for convolutional object detectors, namely that many trees objects are small relative to the image size, and that tree objects are often spatially close. Detection of small objects for proposal-based methods, which are a class of convolutional object detectors to which Faster RCNN belongs, has been shown to be worse than detection on medium objects (Huang *et al.*, 2017). Since these networks downsample each image into a latent feature space before attempting to detect objects, these small objects may not appear in the feature space. This problem is exacerbated with grouped objects, since multiple objects in image space can be reduced to a single

object in feature space (Hu and Ramanan, 2017). Previous work has explored ways to mitigate these problems, including expanding the range of bounding box anchors (Eggert *et al.*, 2017), or preforming data augmentation to change the scale of objects (Hu and Ramanan, 2017). Even with these improvements, performance for small objects from proposal based convolutional object detectors still lags behind performance on large objects (Huang *et al.*, 2017). (Li *et al.*, 2016) explored the use of a sliding window convolutional object detector for tree crown detection, which outperformed other similar tree crown detection techniques. (Hu and Ramanan, 2017) proposes using detections at multiple scales to detect small faces in imagery. Further work incorporating this recent work in small object detection would likely improve metrics for tree crown detection in remote sensing.

2.4.3 Tree Crown Detection

In this paper, we examined the benefit of adding a CHM generated by a GAN to an existing tree crown detection method. We chose the multi-scale watershed segmentation due to its success in tree crown detection in 2D (Wang *et al.*, 2004) and 3D spaces (Zhen *et al.*, 2016). When comparing the multi-scale watershed segmentation between 2D and 3D data, we observed that 2D data tends to lead to a relative overprediction of tree crowns. This overprediction is due to the lack of height data that allows for thresholding of vegetation types. Without any height context, 2D data will classify all vegetation in an area as a potential tree crown, as opposed to only woody vegetation. This overprediction by the 2D dataset is not matched by a similar underprediction by the 3D dataset, as evidenced by the F1 metric (Table 5).

Although we show that Faster RCNN outperforms the multi-scale watershed segmentation algorithm, even with the addition of 3D data, convolutional object detectors present many challenges for accurate detection. First and foremost is the generation of ground truth data. Generating bounding box data for this study took approximately 48 skilled operator hours. When comparing to a method like the multi-scale watershed segmentation, which requires no manual ground truth data creation, the time required to increase accuracy may not be worth pursuing.

2.5 Conclusion

In this study we apply two different individual tree crown detection methods to the problem of detecting woody vegetation, mainly western juniper, in eastern Oregon. The first method is based on a convolutional object detector, specifically Faster RCNN, which was tuned to detect tree crowns within our study area. The second method generated a canopy height model using a generative adversarial network, which was used as an additional predictive input for a multi-scale watershed detection method. We demonstrate the effectiveness of this additional input, in comparing to only using 2D data for tree crown detection, showing approximately 15% improvement in multiscale watershed detection F1 score when using 3D data (Table 5). We aggregate the detections for comparison with the existing work focused on western juniper detection, and we found that the Fast RCNN reduced tree identification errors by almost half. We believe that use of a generative network for estimating three dimensional characteristics of a forest stand has many potential applications in the forestry field, including tree measurement and improvement of existing methods of canopy metric estimation. In addition, we find the results given

by Faster RCNN to be very encouraging for future study in the application of convolutional object detectors to tree crown detection, and object detection in remote sensing in general.

3 Individual Tree Harvest Strategies for Landscape Level Planning using Western Juniper in Oregon

3.1 Introduction

Western juniper (*Juniperus occidentalis* Hook.) is a native, invasive species in Oregon. Remediation of western juniper is an important step for watershed and habitat restoration in many areas of eastern Oregon, where extent of juniper savannahs, defined as having any amount of western juniper canopy cover, has increased more than five times since 1938 (Miller and Rose, 1995). Currently, western juniper is remediated using techniques typical to invasive species remediation, including burning and manual felling. In the past few decades, progress has been made on establishing mills capable of processing the western juniper and its complex tree shape (Swan *et al.*). With the establishment of a potential demand for western juniper, harvesting as a remediation technique becomes feasible, with the possibility of the profit of harvesting offsetting some of the cost of remediation. In order to perform a harvest, a harvest system(s) must be specified, a harvest schedule must be devised - where trees to be harvested, infrastructure to be constructed, and some estimate of costs and values of the harvest are identified.

Applying traditional stand level tree harvest scheduling to western juniper is challenging for a number of reasons. First, given its sparse stand structure and varying stand density, it is difficult to create homogeneous stands which stand level harvesting requires. The complex terrain it thrives in also plays a factor in this varied

stand structure and is especially stark in the Pine and Bridge Creek watersheds in which our study area is located. We have also found during the course of our study that many junipers cannot be profitably harvested, due to the lack of merchantable wood volume within those trees to offset the costs associated with harvesting. Consideration of individual trees allow us to optimize for harvest profitability by accepting solutions which exclude trees that are unprofitable to harvest. Therefore, the objective of this study is to develop a harvest scheduling method that considers the individual tree as elementary management units. This granularity allows us to plan harvest schedules in a much more flexible manner, and in such a way that we can adapt the harvest plan to areas of high or low stand density, and varied stand structure.

3.2 Methods

3.2.1 Study Area

We have selected two areas of approximately 1,600 ha in Wheeler County, Oregon, to test the tree level harvesting strategies developed in this study (
Figure 7); Pine Creek, with an elevation gradient of approximately 500 m, and Bridge Creek with an elevation gradient of approximately 600 m (Table 6). We have chosen the two areas to represent the landscape complexity and distribution of the junipers of Wheeler county as a whole.

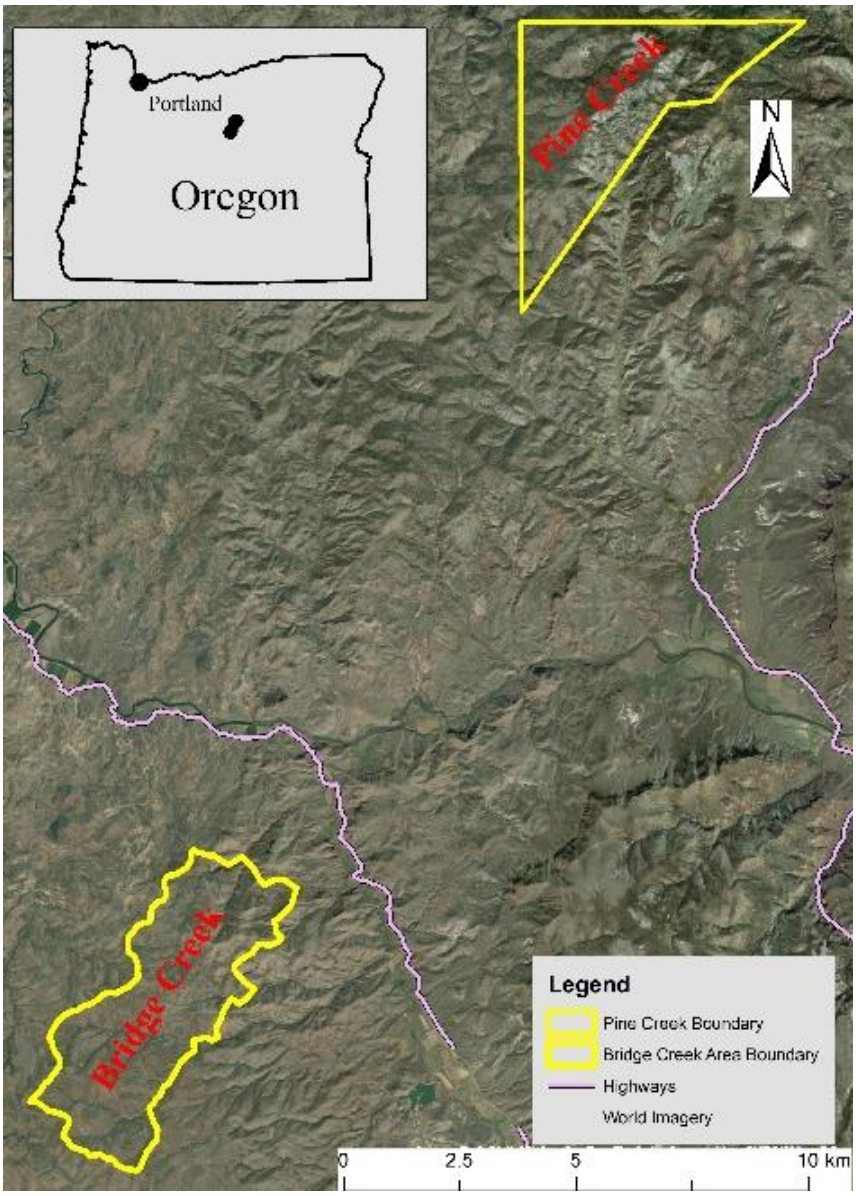

Figure 7. The study areas overlaid on NAIP image (true colors)

The soils present in the two basins are mainly Mollisols, from the Palexerolls and Argixerolls Great Groups (Soil Survey Staff, 1999). The climate is predominantly semiarid warm continental, according to Thornthwhite classification, with average temperature of 11.3°C (hottest month 30.5°C and coldest month 5.5°C), average rainfall 390 mm, and average snowfall of 150 mm. The detailed Koppen-Geiger classification places almost all of Wheeler county in two climates, one warm temperate (i.e., Cfa and Csa – Temperate (C) with hot summers (a) that can be

without dry season (f) or dry summer (s)) and one arid (i.e., BSk – Arid (B) steppe (S) cold (k)). The main tree species growing in these edaphic and climatic conditions is western juniper.

Table 6. Summary statistics describing the two areas

Study Area	Surface	Elevation Mean / min ↔ max / std.dev	Roads length	# sub-basins
	[ha]	[m]	[km]	[count]
Bridge Creek	1667.9	950 / 642 – 1259 / 178.4	21.9 km	12
Pine Creek	1597.1	1133 / 833 – 1358 / 95.7	19.4	14

To identify each tree we used the NAIP multispectral imagery supplied by the USDA (USDA Aerial Photography Field Office, 2015) and two lidar derived products provided by the Oregon Department of Geology and Mineral Industries; namely the digital surface model and the digital terrain model. Lidar collected from the Pine Creek area was used to create a model for generating a canopy height model. This canopy height model was used, along with the multispectral imagery, to provide individual tree locations. The lidar data collected for the Pine Creek site was indirectly used for model creation, but not directly used in this study. No freely available lidar data exists for the Bridge Creek study area.

We used terrain data to ensure that the solutions take into account the complex terrain that dominates the study sites, which can make moving equipment required for harvesting and processing western juniper difficult (Dodson, 2010). We use the 10 meter resolution DEM provided by the USGS (Archuleta *et al.*, 2017) to estimate

basins for individual trees and landing locations. We delineated the watershed with the D8 flow direction model (O'Callaghan and Mark, 1984). The sub-basins of this model are chosen based on segment length threshold (O'Callaghan and Mark, 1984). This resulted in 14 sub-basins for the Pine Creek area and 12 sub-basins for the Bridge Creek area.

3.2.2 Input data

3.2.2.1 Individual Tree Location and Value

A full survey of tree locations was performed using Faster RCNN, applied to the multispectral imagery provided by NAIP (USDA Aerial Photography Field Office, 2015). The algorithm estimated the spatial coordinates of approximately 175,000 trees in the Pine Creek area and approximately 160,000 trees for the Bridge Creek area. Positional information was combined with a canopy height model. The height model was derived using a generative adversarial network trained on a lidar data collected from a region of similar terrain and tree species distribution. The canopy height model allowed us to estimate tree height, which was on average 27 feet for Pine Creek Area and 19 feet for the Bridge Creek area (Table 7). The algorithm did not identify the tree species for each detected tree; however, field survey and random NAIP images analysis revealed that more than 90% of the trees were western juniper, with only a small portion being other species, mostly ponderosa pine. Although other species are present on the study areas, for simplicity we considered that all trees are western juniper.

Table 7. Summary statistics for the predicted tree height and value

Study area	# trees	Height Mean / Min - Max	Std. dev
	[count]	[ft]	[ft]
Pine Creek	178515	27.09 / 6 -119	14.70
Bridge Creek	162941	19.04 / 6 - 80	8.29

To represent the value of an individual juniper tree, we have harvested a set of 26 western juniper trees, which were processed at the "In The Sticks" sawmill at Fossil, OR The trees were selected randomly, the focus being on stems that provide revenue, measured as merchantable timber. Therefore, to estimate the value of each tree, first we computed the merchantable volume of each stem, in cubic feet, then we developed a linear model that relates the volume with the total height of juniper (Equation 5)

$$Volume_{juniper} = 0.82 \times height_{juniper}$$

Equation 5. Equation relating juniper height in feet to merchantable volume in cubic feet

Although the final product sold by the mill is square timber, the wood is acquired using weight. Therefore, from landowner's perspective green weight is the measure used to estimate potential value of harvested juniper. This value is estimated at $65 per US ton (Derby, 2018). We converted the volume from Equation 5 to weight assuming a density of 31 lb/cf, as estimated by Swan and Connolly (1998). Since this density assumes a moisture content of 12%, which is lower than would be in a freshly felled juniper, we convert to a moisture content of 45% to approximate the green weight of each log. For our weight computation, we assume a density of 49.91 lb/cf. These equations were used during a data preprocessing step in order to convert estimated juniper height to estimated merchantable value.

We split each juniper into two categories based on weight, those which will be harvested and sent to a mill for processing, and those which will be felled and left in the field. Many juniper are too small to be harvested profitably, due to junipers challenging morphology (Gedney *et al.*, 1999). However, these trees are still valuable

from an ecosystem services sense, and this value is recognized by the USDA which has provided grants for juniper remediation (cutting). Western juniper which are harvested have this value, in addition to the potential merchantable timber value. Each juniper is determined to either be a harvestable or non-harvestable tree, based on a weight threshold. Only western juniper above a certain weight threshold contain enough merchantable volume to be profitably harvested, so we split trees into two categories. This weight threshold for western juniper was determined to be 0.3 metric tons, based on the costs of felling, processing, and skidding described in (Dodson, 2010), to ensure that all processed trees would be profitable, given the costs of processing and the revenue of selling a processed log. All trees below 0.3 metric tons only had felling costs and the remediation value modeled, whereas all trees above 0.3 metric tons had felling, processing, and skidding costs, as well as remediation and harvest value. The values were determined using the estimated tree weight but split into categories to deal with the problem of modeling trees whose size prevents them from being profitably harvested.

Given that the value of juniper is determined almost entirely by the merchantable volume calculation, we also investigated the effect of a different value per ton of juniper. For this investigation, we used a value of $45 per ton.

3.2.3 Landing Locations

Landing locations are truck accessible points where logs can be loaded onto trucks for transport to the mill. Logs are skidded from their felling point to a landing. Potential landing locations were determined from the improved and unimproved road network (Table 8). The improved roads in the two study areas are gravel roads that are

constantly maintained, while the unimproved roads are roads with limited or no maintenance (Figure 8 a, c). The unimproved tracks were digitized from the NAIP aerial imagery in ArcGIS 9.3 (Environmental Systems Research Institute, 2008). The potential landings were relatively evenly distributed along the road network, approximately 150 feet apart. In addition to the existing roads, we have digitized the location of other possible landings (Figure 8 b, d) using four criteria: 1) increasing accessibility to western juniper, 2) the possibility to connect unimproved and improved roads, 3) realistic positioning on the slope and landscape, and 4) ensuring a distance of approximately 150 feet between landing locations.

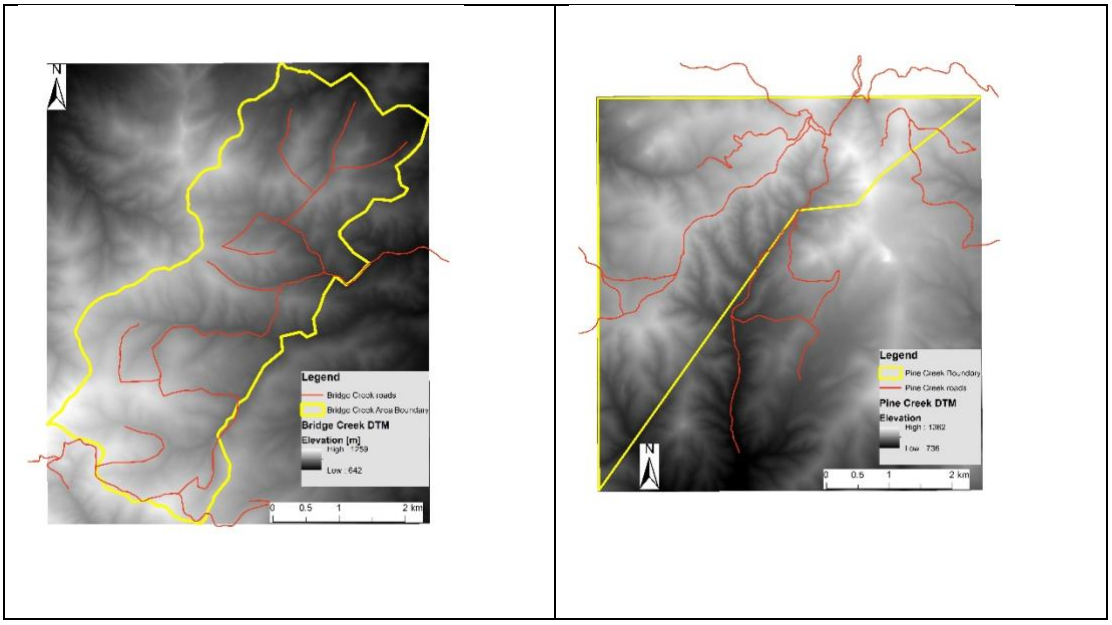

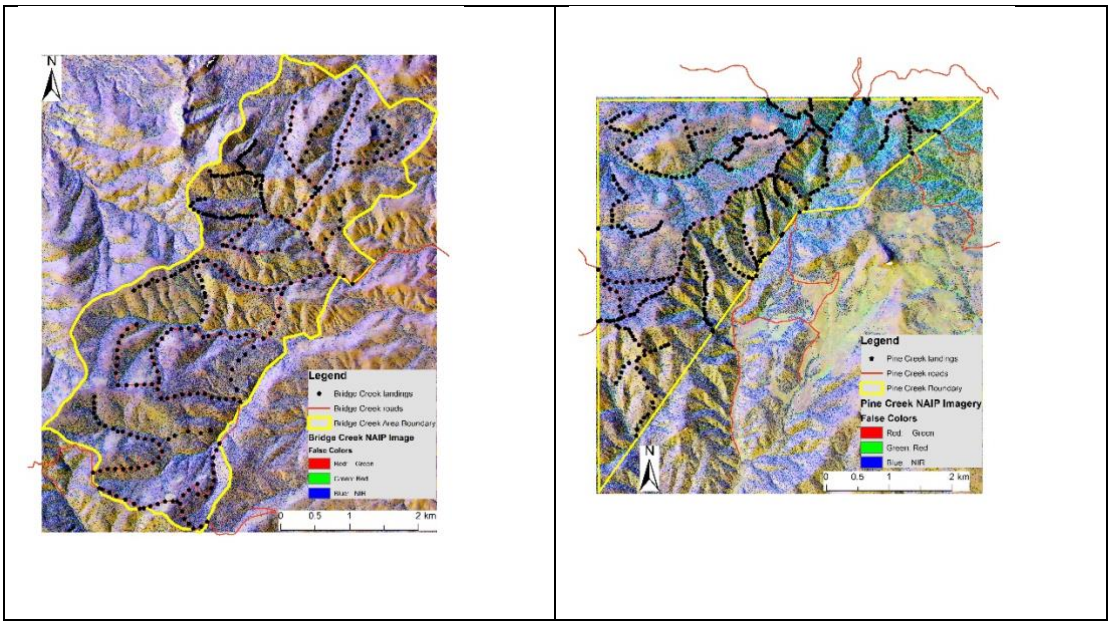

Figure 8. Road network and landings for the two study areas overlaid on the digital terrain model: a) road network of the Bridge Creek area, b) landings for the Bridge Creek Area, c) road network of the Pine Creek area, d) landings for the Pine Creek Area

Table 8. Summary statistics for the possible landings

Study area	# landings	Average area / landing [ha]
Bridge Creek	344	4.6
Pine Creek	399	4.2

3.3 Individual Tree Harvest Scheduling Optimization

Spatial explicit forest planning problems using stands as an elementary management unit have polynomial complexity (Bettinger *et al.*, 2003). Tree level forest planning problems can be considered from the view of each stand consisting of a single tree, which demonstrates that tree level harvesting is also polynomial in complexity. Considering that each individual tree and landing location is a distinct decision variable, the scale of this problem suggests heuristic methods rather than linear programming. To process the large number of possible solutions that select the trees

to be harvested in a feasible computation time, we explore the use of two Monte Carlo based optimization heuristics: simulated annealing (Metropolis *et al.*, 1953; Kirkpatrick *et al.*, 1983) and record to record travel (Dueck, 1993). This class of optimization techniques have shown good results for tree harvest scheduling (Bettinger *et al.*, 2003), and are noted for their solution quality and ease of implementation in comparison to other heuristic optimization techniques. Monte Carlo methods are based on a neighborhood search, where each solution is a modification of a previous solution. By choosing these modifications wisely, we can efficiently search the problem space to find a near-optimal solution. Our problem is combinatorial in nature, in that we must simultaneously find a set of trees and landing sites which optimize profit.

Our optimization criteria are based on solution profitability, which is represented as the sum of the values of each tree scheduled to be harvested, minus the costs associated with harvesting of those trees including development of landing sites and transport costs. We were interested in modelling these values and costs to produce a realistic harvesting plan for our two areas. The cost and revenue for each tree depends on two variables, the weight of the tree and distance from the tree to the closest active landing. We model two scenarios for each area, one assuming the area is very close to the mill, and one that assumes the area is farther from the mill.

3.3.1 Harvest Costs

Modeled costs are based on the work of Dodson (2010), which examined a series of potential harvest systems for western juniper in eastern Oregon. Felling and processing costs are both based on tree weight, and skidding weight is based on a

combination of tree weight and distance to landing. To enforce a maximum distance constraint for small trees, which are only felled for their USDA remediation value, we also model equipment moving cost, which is based on distance to the centroid of each proposed harvest unit.

One of the most important concerns in forest harvest scheduling is distance from the proposed harvest units and the potential landing locations. For our project, we started with a Euclidean distance metric to measure the distance between the coordinates of the harvest unit centroid and the landing point coordinate. However, the study areas contain challenging terrain which would be difficult to traverse for some forest harvest machinery, and whose cost would not be modeled in a simple Euclidean distance. To avoid crossing large ridges, we segment the study areas into basins, using a sub-watershed segmentation adapted from (Wang *et al.*, 2004). Crossing between basins is a good indicator that a significant terrain change has occurred. Therefore, we add the basin identifier as component to the coordinates for both the landing points and harvest units. If a change in basins between a landing and harvest unit occurs, then a significant cost is applied, which will encourage the heuristic to select a different landing point or abandon that harvest unit. For our algorithm, we found a distance penalty of 10,000 feet to be sufficient to ensure that harvest units were not assigned to landings outside of their basin.

Each landing location also has an associated fixed cost. Land acquisition costs were not considered, so the cost is defined by the creating of a landing, which was estimated at $500 (Sessions, 2018).

3.3.2 Spatial implementation of the harvests

Spatial considerations in scheduling harvests is focused on constraining the harvest such that a large opening does not occur. Achievement of this constraint is commonly implemented with three approaches (St. John and Tóth, 2013): restricting neighbors for harvest once an elementary management unit is cut, as in the unit restricted model, restricting the size of the cut, as in the area restricted model, and a combination of difference equation. However, our study is not limited by the size of the harvest, as the purpose of the study was landscape restoration by removing all possible juniper. To clear an area as large as possible we started by defining the smallest area on which harvest can occur. We can naturally define such an area, which serves as an elementary planning unit, by referring to the capabilities of the devices executing the harvests. For juniper logging will be most likely executed with a excavator-based, feller-buncher, which can reach trees at most 25 feet from the operator (Dodson, 2010). If a rubber-tired drive-to-tree feller buncher is used, we assume the same collection distance. Therefore, we define an elementary planning unit as a square with side length of 50 feet. The elementary planning units create a grid with the cell size of 2500 ft^2. We should point out that even though a grid is used for harvesting, scale is not a part of the analysis, as the cell size is defined by the forest operations, and not analytically. Furthermore, no spatiality or generality is lost as all the trees within a cell will be harvested from one location, the center of the cell.

Trees within each grid cell are aggregated and used for optimization. Each grid cell is a harvest unit. After aggregating all trees into grid cells, we reduce problem complexity by not including the harvest units with costs that exceed the value of the

trees. If a harvest unit is not profitable, even assuming the closest possible landing point, then it is removed from the set of eligible harvests.

In order to use a heuristic to find the optimal solution for a problem, we must first define the problem space, and the method by which the heuristic will move through it. In our problem, we have only two sets of decision variables, the set of active harvest units (ahu), and the set of active landings (al). With these sets of decision variables, our movement through the problem space is simple, we can move a harvest unit between the active and inactive set or move a landing point between the active and inactive set. For our problem formulation, we enforced that the active landing set must always contain at least one member, that is, if there was only one element in the active landing set, there was no way to move that active landing into the inactive set. The set of active harvest units and landing points make up a solution. Each solution has all the required information for the objective function, which is used by the heuristic to determine if the move chosen though the solution space was effective. For each possible move, we also define a probability for that move occurring. We determined this probability through trial and error; however we followed a basic intuition about the frequency we would like these moves to occur in relation to each other. When selecting a possible move, we compare a random uniform number in the set (0, 1] to this probability, and choose the move if the random value is less than the probability. In this way, over 200,000 total moves, these values form a probability of a type of move occurring, in relation to the other possible moves.

- Move harvest unit from inactive to active set 1.0
- Move harvest unit from active to inactive set 0.5

- Move landing from inactive to active set 0.1
- Move landing from active to inactive set 0.1

Modifying these probabilities determines the general class of a solution, w

3.3.3 Record to Record Travel

Record to Record Travel (R2R) is an optimization heuristic which focuses on only allowing the current solution to exist within certain range of deviation from the best observed solution (Dueck, 1993).This method is conceptually similar to the naive hill climbing heuristic, with the difference that deviation for selection of non-optimal solutions are allowed. The major advantage of R2R over other heuristic methods is the reduced number of parameters to tune; only two, namely the amount of deviation allowed and the ending of the algorithm. To find the values suitable for our problem we used a trial-and-error approach, common in application of heuristic techniques (Strimbu and Paun, 2012). We found that a deviation of 10% from the best observed solution and an exploration of 200,000 moves supplies acceptable solutions. We also implemented an additional stopping rule based on non-improvement of the solution. If the best solution does not improve after 10,000 moves, or 5% of the total possible moves, we terminate the heuristic under the assumption that the optimum value for this run has been reached. In order to avoid premature termination, we only enforce this stopping condition after 150,000 moves. At the termination of the algorithm, the best solution was chosen as the output of the heuristic. Being heuristic, R2R can supply close to optimal or far from optimal solutions. Consequently, we have executed a set of 29 runs for each study area, which we expect will render solutions

close to optimality. A pseudocode description of the R2R implementation which we choose is shown below.

```
moves since last improvement = 0
minimum moves before termination = 150000
non-improving moves before termination = 10000

maximum moves = 200000
allowed deviation = 0.1

move
    if continue_solving
        if accept_solution
            current solution = proposed solution

            if proposed solution > best solution
                best solution = proposed solution
                moves since last improvement = 0

        increment moves since last improvement


continue_solving
    if current moves > maximum moves
        do not continue solving

    if current moves > minimum iterations before moves and
       moves since last improvement > non-improving moves before
termination
        do not continue solving

    continue solving

accept_solution
    if proposed solution > best solution - abs(best solution *
allowed deviation)
        accept proposed solution
    else do not accept proposed solution
```

Figure 9. Psuedocode for Record to Record implementation

3.3.4 Simulated Annealing

Simulated Annealing (SA) is a heuristic technique based off the idea that the allowable negative deviation from the current solution should decrease over the number of iterations (Metropolis *et al.*, 1953; Kirkpatrick *et al.*, 1983; Van Deusen, 1999). This heuristic follows the analogy of physical properties of a metal as it cools

during an annealing process. Early in the cooling process, molecules are driven by the energy required by annealing and are able to move substantially, but later in the cooling process this energy is reduced, and molecules move much less. SA is mathematically represented through an exponential function and a 'temperature' variable, which allows for large negative deviation for high temperatures, and only small negative deviation when the temperature is small. SA is driven by at least four parameters (Bettinger *et al.*, 2002): annealing rate, initial temperature, number of moves at each temperature, and the stopping rule. The acceptance of a non-improving solution is analogous to reheating the metal. Identification of proper parameters has a significant role on SA performance. We have chosen the parameters by trial-and error, which are:

- Annealing rate: 0.99
- Initial temperature: 0.25
- Number of moves/temperature: 200
- Stopping rule: freezing temperature of 0.00001 or no improvement for 10,000 moves (~5% of the possible moves), whichever occurs first. If SA reaches the freezing temperature 201,000 moves were executed.

We found that normalizing the deviation between neighboring solutions by the current solution value provided the consistent results. This normalization, which bounded the solution fitness deltas between -1 and 1, is the reason for the low initial temperature. The full description of the SA implementation which we chose, including the normalization, is shown in pseudocode below. To mirror the results of R2R we have executed 29 SA runs for each study area.

```
moves since last improvement = 0
minimum moves before termination = 150000
```

```
non-improving moves before termination = 10000

current temperature = 0.25
alpha = 0.99
repetitions per temperature = 200
minimum temperature = 0.00001

move
    if current move % repetitions per temperature is 0
        current temperature = current temperature * alpha

    if continue_solving
        if accept_solution
            current solution = proposed solution

            if proposed solution > best solution
                best solution = proposed solution
                iterations since last improvement = 0

        increment iterations since last improvement


continue_solving
    if current temperature < minimum temperature
        do not continue solving

    if current iterations > minimum moves before termination and
    moves since last improvement > non-improving moves before
termination
        do not continue solving

    else continue solving

accept_solution
    normalized fitness delta =
        (current solution - proposed solution) /
        (abs(current solution) + abs(proposed solution))

    accept probability = 1.0 / exp(normalized fitness delta /
temperature)

    if random uniform value (0, 1] < accept probability
        accept proposed solution
    else do not accept proposed solution
```

Figure 10. Psuedocode for Simulated Annealing implementation

3.3.5 Harvesting problem formulation

The objective function to be maximized is the net revenue obtained from harvesting all active harvest units, and constructing all active landings:

$$max(\sum_{h}^{ahu}(FV_i + HV_i) - (EQMC_i + FC_i + PC_i + SKC_i) - \sum_{l}^{al} LC_i) \qquad 6$$

subject to

$$harvest\ weight = sum\ of\ weights\ of\ trees\ with\ weight > 0.3\ tonnes$$
$$non\ harvest\ wieght = sum\ of\ weights\ of\ trees\ with\ weight \leq 0.3\ tonnes$$
$$distance\ to\ closest\ active\ landing = euclidean\ distance\ from\ centroid\ of\ harvest\ unit,\ in\ feet$$

Each active harvest unit, defined as the h^{th} value in the active harvest unit set:

- Does not belong to the inactive harvest unit set

Has a fitness value > 0 when assigned to the closest possible landing location, where the harvest unit fitness is defined by the values and costs in

- Table 9.

Each active landing, defined as the l^{th} landing in the active landing set:

- Does not belong to the inactive landing set

where

Constant	Value	Units	Short Description
Felling constant	2.0	dollars/tree	Estimated USDA remediation value (Magenheimer, 2011)
Harvest value constant	71.65	dollars/metric ton	Estimated value of tree at mill (Derby, 2018)
Equipment Moving constant	0.01	dollars/foot	Estimated cost of moving equipment to harvest unit (Sessions, 2018)
Non-harvest felling constant	12	dollars/metric ton	Cost of felling a non-harvested tree (Dodson, 2010)
Harvest felling constant	10	dollars/metric ton	Cost of felling a harvested tree (Dodson, 2010)
Processing constant	15	dollars/metric ton	Cost of processing a harvested tree (Dodson, 2010)
Skidding Distance constant	0.061	dollars/foot * metric ton	Cost of moving juniper to the landing (Dodson, 2010)

Skidding Weight constant	20	dollars/metric ton	Cost of moving juniper to the landing (Dodson, 2010)
Landing constant	500	dollars/landing	(Sessions, 2018)

Table 9. Juniper harvest cost and value constants

$$number\ of\ active\ harvest\ units\ (ahu)$$
$$number\ of\ active\ landings\ (al)$$

$$felled\ value\ (FV) = number\ of\ trees\ in\ harvest\ unit * felling\ value\ constant$$
$$harvested\ value\ (HV) = harvest\ weight * harvest\ value\ constant$$

$$equipement\ moving\ cost\ (EQMC) = distance\ to\ closest\ active\ landing * equipment\ moving\ constant$$
$$felling\ cost\ (FC) = non - harvest\ weight * non - harvest\ felling\ constant + harvest\ weight * harvest\ felling\ constant$$
$$processing\ cost\ (PC) = harvest\ weight * processing\ constant$$
$$skidding\ cost\ (SKC) = harvest\ weight * (distance\ to\ closest\ active\ landing * skidding\ distance\ constant + skidding\ weight\ constant)$$
$$landing\ cost\ (LC) = landing\ constant$$

3.4 Results

An upper bound for the objective function can attain is $559,281 for the Pine Creek area and $289,752 for the Bridge Creek area, under the assumptions that each harvest unit will travel to the closest possible landing, harvest units with negative values after this step are removed, and that no costs for landings are assumed and the transport cost to the mill is zero. Given this value, the baseline naïve solution would be obtained with every landing with a positive value in the active harvest set, and all possible landings in the active landing set and the transport cost is zero. This naïve value can be obtained by subtracting the costs of all landings from the largest value, which equal $359,781 for Pine Creek area and $117,752 for the Bridge Creek area. The results of the 29 runs show the existence of a large number of solutions below the lower bound for each area and both algorithms (Table 10).

Table 10. Summary statistics of the 29 runs at $65 per ton

Study area	Algorithm	Maximum value	# solutions above lower bound	Stopping of best solution
Bridge creek	SA	154,943	23	freezing
	R2R	125,464	23	Non-improvement
Pine Creek	SA	397,219	12	freezing
	R2R	365,836	19	Non-improvement

The top solutions revealed consistent results, with the R2R terminating because the solution did not improve for more than 10,000 moves whereas SA ended when the freezing temperature was reached (Figure 11). Nevertheless, for both areas the SA solutions did not improve more than 1% for the last 40,000 moves, which suggests that increasing the number of moves will not significantly improve the objective function.

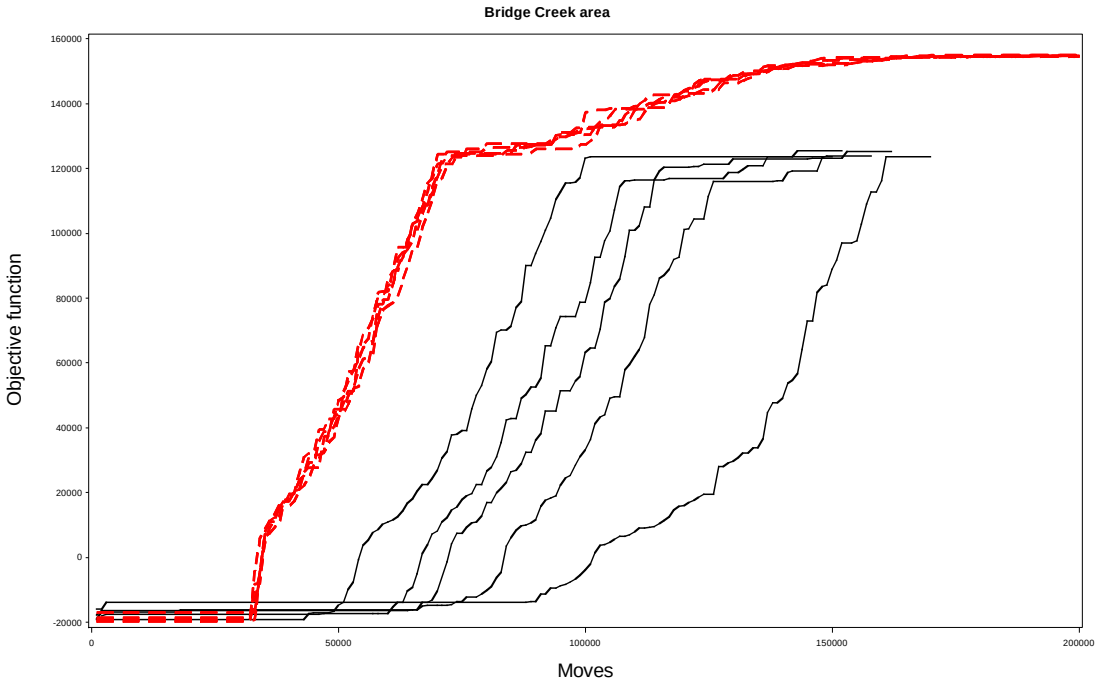

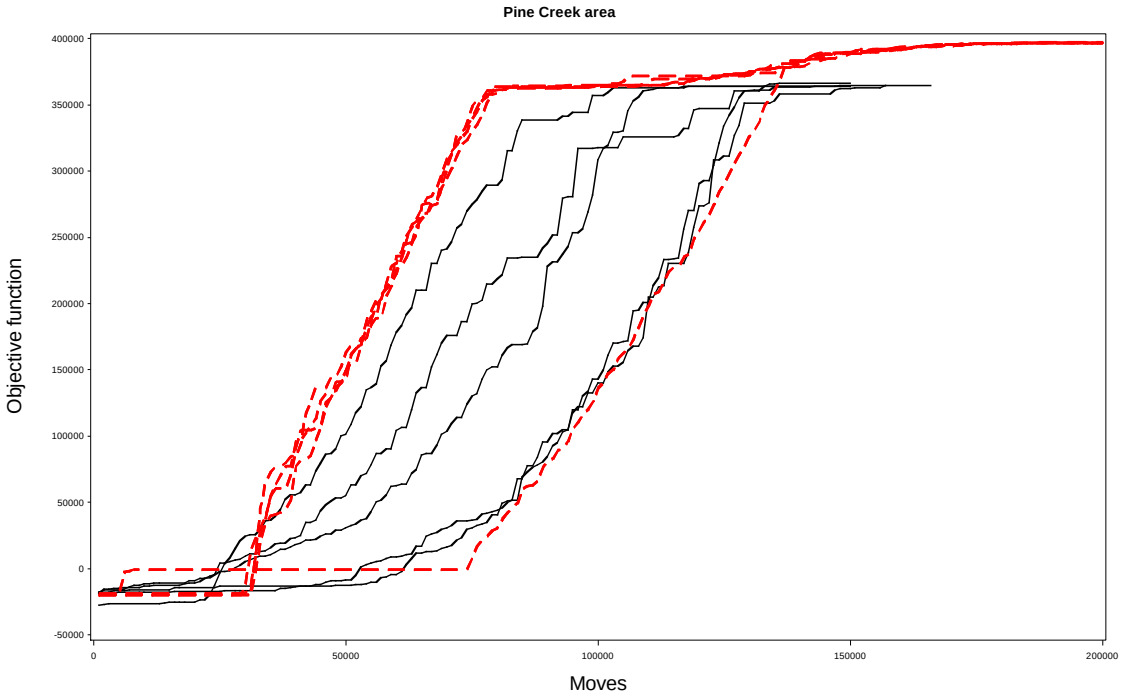

Figure 11. Improvement of the solution with the number of moves at $65 per ton: a. Bridge Creek area b. Pine Creek area

For both algorithms and study areas, the best solutions revealed that the average weight reaching a landing is more than 20 tons, which is the expected load of one truck (Table 11). We also see that the best R2R solution had significantly more landings than the solutions chosen by SA, which contributed to the lower per landing averages for the harvest unit metrics.

Table 11. Summary statistics describing the best solution for each area and algorithm

Study area	Heuristic	# landings	Average weight/ landing	Average distance from cell to landing	Average # cells/ landing	Average# trees harvested/ landing
		[count]	[metric ton]	[ft]	[count]	[count]
Bridge creek	SA	223	90	233	94	228
	R2R	308	65	214	68	201
Pine Creek	SA	260	293	236	171	550

	R2R	354	108	224	63	202

We also computed a smaller set of statistics for the runs working off a value of $45 per ton (Table 12). Additional graphs showing the fitness of each run at steps of 1000 moves is shown in Figure 12.

Table 12: Summary statistics of runs at $45 per ton

Study area	Algorithm	Maximum value
Bridge creek	SA	-461
	R2R	-486
Pine Creek	SA	17,468
	R2R	17,315

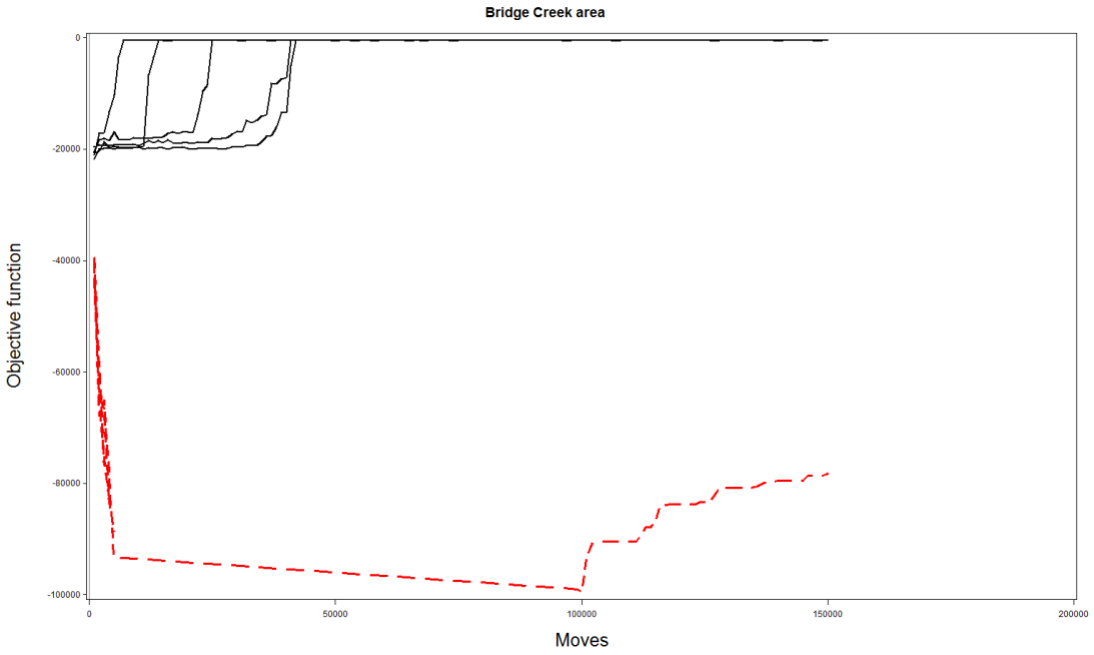

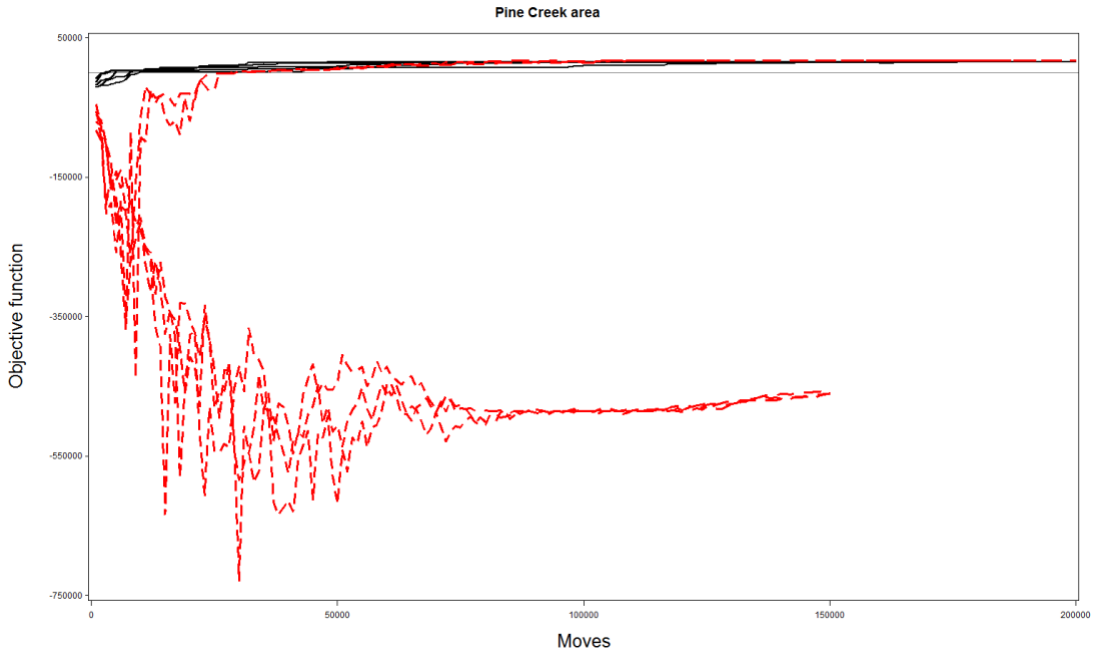

Figure 12: Improvement of the solution with the number of moves at $45 per ton: a. Bridge Creek area b. Pine Creek area.

3.5 Discussion

Overall, for the grid-cell based method, we see that the solutions are separated into two main classes, and that the values for the top five solutions are internally very consistent. The two classes we see the solutions forming are those which are located close to the global optima, and those which became trapped in a local minimum. Of those solutions which became trapped in a local minimum, a frequent occurrence was obtaining a solution which contained only one active landing, and a small number of cuts which would be optimally harvested to that landing. This was a common solution case due to the fixed cost of establishing a new landing, which was $500, and the heuristic formulation which only allowed a percentage deviation from the current solution fitness. If the fitness of the current solution was near zero, the heuristic was unlikely to choose a solution with an additional landing, due to the fact that the fixed landing cost would often exceed the allowed deviation from the current solution.

We also see in our results some solutions which are below, but close to, the baseline value. In this case, the solution was trapped in a local minimum for the first 100,000 iterations. The solution reached a plateau near the 150,000 iterations and was terminated around iteration 160,000 because of the stopping rule which terminates a run after 10,000 iterations without improvement. If this rule had not been in place, it is likely that this solution would have exceeded the baseline value and been closer to the rest of the solution class which were closer to the local optima.

We observe that SA performs 10 to 20% better than R2R travel for this problem formulation. We believe that the weak performance of R2R in respect with SA is due to the fact that the R2R runs were more likely to terminate with the non-improvement stopping rule, than reaching their maximum iterations. This indicates that the R2R runs were more likely to be trapped in a class of solutions which were a local minimum, and which have more active landings in the final landing set. This outcome is likely due to the complexity and number of steps required for the heuristic to remove a landing in our algorithm formulation. Later in the run, when more and more harvest units are in the active set, removing a landing can mean a significant cost increase, as all harvest units whose closest landing was removed are re-assigned to their new closest landing, which can be much farther away. We mitigated this case by allowing these harvest units to have zero fitness for a small number of moves, or until a closer landing was activated. However, even with this allowance, removing a landing can lead to a loss of fitness if the value of all associated cuts is greater than the cost of a landing, even if this temporary loss of fitness could lead to a better

overall solution. From these results, we concluded that R2R was not able to explore the very large solution space as effectively as SA.

From the experiments with the reduced value per ton of western juniper, we see that the value per ton has a significant effect on the final solution value. Given that this is the main driver of juniper value, this is to be expected. This dramatic drop off in solution value with a 30% reduction in juniper value per weight shows that even a smaller change in juniper value may have a dramatic effect on the overall profitability of harvesting. We also assume in this paper that the $65 per ton is the at landing value, as opposed to the at mill value, since we do not model transportation costs from the landing to the mill. This $45 per ton estimate can also be viewed as a surrogate for modelling the value at the mill, when removing the costs of transporting from the landing to the mill. We can see that a study site which is a significant enough distance from the mill will likely have similar results to the solutions generated assuming $45 dollars per ton.

3.6 Conclusion

Western juniper poses a number of challenges to harvest scheduling. However, harvest scheduling is an important step towards viewing western juniper as a merchantable resource, as opposed to an invasive species. We have demonstrated a procedure, based on tree harvesting systems, of aggregating individual trees into elementary harvest units. In addition, we have formulated an algorithm which defines the solution space for working with these harvest units in a harvesting context, including felling, processing, and skidding to a set of potential landings. This approach proved robust to difficult terrain, and a large number of decision variables.

Two areas of similar size and terrain but with far different tree distributions were defined. We applied two heuristics, simulated annealing and record to record travel, to this algorithm, in order to optimize the fitness for our current objective of profitability. These heuristics produced results with a greater fitness than the baseline naïve solution in almost all non-trivial runs. Ultimately, we found that the complexity of the solution space lead to simulated annealing outperforming record-to-record travel in both of our study areas. Through this example problem formulation, we demonstrate that our algorithm and solution space definition could be applied to similar problem sets where complex stand structure preclude the use of traditional stand level harvest scheduling, and instead require a more granular system.

The two scenarios, (i) negligible truck transport costs, and (ii) significant transport costs suggest that the positive solutions are highly dependent on the transport distance. The farther the landing is from the mill, the closer to the landing the juniper tree must be to be viable.

3.7 Future Work

Future work should include transportation from the individual landing to the mill. The small volumes per landing in these examples, suggest that a self-loading truck might be preferable to a separate loader. Landing costs in this study assumed mobilization of a separate loader. A study of transport distance, truck load capacity with and without the self-loader, and landing mobilization costs for the separate loader will need to be considered.

4 Conclusion

In this work I describe two novel methods that provide essential information for forest decision making: estimation of the available resources and the feasibility of harvesting those resources. This work is focused on the major tree species within our study area, western juniper. I estimated the location of each western within study area inventory using two methods, one based on Faster RCNN and one based on the watershed algorithm. The novelty of my method consists in estimation of three-dimensional data in the form of a canopy height model from two dimensional, multispectral images. I found that the convolutional neural network outperforms the classical watershed algorithm for tree crown detection for our study area. My findings show that the accuracy of my individual tree crown detection methods is superior to the existing work, which is based on a fixed grid scale. The most important contribution of my work is development of a method that allows tree height measurement for every detected tree crown using multispectral images.

The tree height estimated from 2D data serves as inputs in an allometric relationship that computes tree weight and merchantable value. Based on the estimated value distributed spatially on the landscape, I developed a method for scheduling tree harvests. The method is novel contribution to the field of harvest scheduling, which is historically focused on stand level harvesting, whereas my method is tree level centered. This method allows for harvest scheduling for unmanaged stands, or forest composed primarily from uneven aged-multispecies stand with medium to low density. I believe that the tools that I developed will be useful for western juniper

remediation, as well as provide valuable information to decision makers that manage forests with similar ecological and geographical parameters.

Archuleta, C.-A.M., Constance, E.W., Arundel, S.T., Lowe, A.J., Mantey, K.S., Phillips, L.A., 2017. The National Map seamless digital elevation model specifications. In. US Geological Survey.
Avery, T.E., Burkhart, H., 2015. Forest Measurements. Waveland Press, Long Grove IL.
Ayrey, E., Fraver, S., Kershaw, J.A., Kenefic, L.S., Hayes, D., Weiskittel, A.R., Roth, B.E., 2017. Layer Stacking: A Novel Algorithm for Individual Forest Tree Segmentation from LiDAR Point Clouds. Canadian Journal of Remote Sensing 43, 16-27.
Azuma, D.L., Hiserote, B.A., Dunham, P.A., 2005. The western juniper resource of eastern Oregon. USDA, Forest Service, Pacific Northwest Research Station.
Bannari, A., Morin, D., Bonn, F., Huete, A., 1995. A review of vegetation indices. Remote sensing reviews 13, 95-120.
Baruch-Mordo, S., Evans, J.S., Severson, J.P., Naugle, D.E., Maestas, J.D., Kiesecker, J.M., Falkowski, M.J., Hagen, C.A., Reese, K.P., 2013. Saving sage-grouse from the trees: a proactive solution to reducing a key threat to a candidate species. Biological Conservation 167, 233-241.
Bengio, Y., Courville, A., Vincent, P., 2013. Representation Learning: A Review and New Perspectives. IEEE Transactions on Pattern Analysis and Machine Intelligence 35, 1798-1828.
Bettinger, P., Graetz, D., Boston, K., Sessions, J., Chung, W.D., 2002. Eight heuristic planning techniques applied to three increasingly difficult wildlife planning problems. Silva Fennica 36, 561-584.
Bettinger, P., Sessions, J., Chung, W., Graetz, D., Boston, K., 2003. Eight heuristic planning techniques applied to three increasingly difficult wildlife planning problems: A summary. In, Systems Analysis in Forest Resources. Springer, pp. 249-257.
Blaschke, T., 2010. Object based image analysis for remote sensing. ISPRS journal of photogrammetry and remote sensing 65, 2-16.
Camps-Valls, G., Tuia, D., Bruzzone, L., Benediktsson, J.A., 2014. Advances in Hyperspectral Image Classification: Earth Monitoring with Statistical Learning Methods. IEEE Signal Processing Magazine 31, 45-54.
Chen, Q., Baldocchi, D., Gong, P., Kelly, M., 2006. Isolating individual trees in a savanna woodland using small footprint lidar data. Photogrammetric engineering and remote sensing 72, 923-932.
Cheng, G., Zhou, P., Han, J., 2016. Learning rotation-invariant convolutional neural networks for object detection in VHR optical remote sensing images. IEEE Transactions on Geoscience and Remote Sensing 54, 7405-7415.
Davies, K.W., Petersen, S.L., Johnson, D.D., Davis, D.B., Madsen, M.D., Zvirzdin, D.L., Bates, J.D., 2010. Estimating juniper cover from National Agriculture Imagery Program (NAIP) imagery and evaluating relationships between potential cover and environmental variables. Rangeland Ecology & Management 63, 630-637.
Derby, K., 2018. In.
Dodson, E.M., 2010. A comparison of harvesting systems for western juniper. International journal of forest engineering 21, 40-47.
Dueck, G., 1993. New optimization heuristics: The great deluge algorithm and the record-to-record travel. Journal of Computational physics 104, 86-92.
Eggert, C., Brehm, S., Winschel, A., Zecha, D., Lienhart, R., 2017. A closer look: Small object detection in faster R-CNN. In, Multimedia and Expo (ICME), 2017 IEEE International Conference on. IEEE, pp. 421-426.
Environmental Systems Research Institute, I., 2008. ArcGIS. In. ESRI, Redlands CA.

Gedney, D.R., Azuma, D.L., Bolsinger, C.L., McKay, N., 1999. Western juniper in eastern Oregon.
Ghamisi, P., Yokoya, N., 2018. IMG2DSM: Height Simulation From Single Imagery Using Conditional Generative Adversarial Net. IEEE Geoscience and Remote Sensing Letters.
Hu, P., Ramanan, D., 2017. Finding tiny faces. In, 2017 IEEE Conference on Computer Vision and Pattern Recognition (CVPR). IEEE, pp. 1522-1530.
Huang, J., Rathod, V., Sun, C., Zhu, M., Korattikara, A., Fathi, A., Fischer, I., Wojna, Z., Song, Y., Guadarrama, S., 2017. Speed/accuracy trade-offs for modern convolutional object detectors. In, IEEE CVPR.
Hulet, A., Roundy, B.A., Petersen, S.L., Bunting, S.C., Jensen, R.R., Roundy, D.B., 2014. Utilizing national agriculture imagery program data to estimate tree cover and biomass of pinon and juniper woodlands. Rangeland Ecology and Management 67, 563-572.
Isola, P., Zhu, J.-Y., Zhou, T., Efros, A.A., 2017. Image-to-image translation with conditional adversarial networks. arXiv preprint.
Jakubowski, M.K., Li, W., Guo, Q., Kelly, M., 2013. Delineating individual trees from LiDAR data: A comparison of vector-and raster-based segmentation approaches. Remote Sensing 5, 4163-4186.
Jeppesen, D.J., 1977. Competitive moisture consumption by the western juniper (Juniperus occidentalis). In, Proceedings: Western Juniper Ecology and Management Workshop. USDA Forest Service General Technical Report PNW-74, pp. 83-90.
Kaartinen, H., Hyyppä, J., Yu, X., Vastaranta, M., Hyyppä, H., Kukko, A., Holopainen, M., Heipke, C., Hirschmugl, M., Morsdorf, F., Næsset, E., Pitkänen, J., Popescu, S., Solberg, S., Wolf, B.M., Wu, J.-C., 2012. An International Comparison of Individual Tree Detection and Extraction Using Airborne Laser Scanning. Remote Sensing 4, 950.
Ke, Y., Quackenbush, L.J., 2011. A review of methods for automatic individual tree-crown detection and delineation from passive remote sensing. International Journal of Remote Sensing 32, 4725-4747.
Kershaw, J.A., Ducey, M.J., Beers, T.W., Husch, B., 2017. Forest Mensuration. Wiley Blackwell, Hoboken NJ.
Kirkpatrick, S., Gelatt, C.D., Vecchi, M.P., 1983. Optimization by simulated annealing. science 220, 671-680.
Längkvist, M., Kiselev, A., Alirezaie, M., Loutfi, A., 2016. Classification and Segmentation of Satellite Orthoimagery Using Convolutional Neural Networks. Remote Sensing 8, 329.
Li, W., Fu, H., Yu, L., Cracknell, A., 2016. Deep learning based oil palm tree detection and counting for high-resolution remote sensing images. Remote Sensing 9, 22.
Long, J., Shelhamer, E., Darrell, T., 2015. Fully convolutional networks for semantic segmentation. In, Proceedings of the IEEE conference on computer vision and pattern recognition, pp. 3431-3440.
Magenheimer, J.M.S., 2011. Landowners Encouraged to Apply Now for Funding to Improve Sage-Grouse Habitat and Manage Juniper. In, NRCS Oregon.
Metropolis, N., Rosenbluth, A.W., Rosenbluth, M.N., Teller, A.H., Teller, E., 1953. Equations of State Calculations by Fast Computing Machines. Journal of Chemical Physics 21, 1087-1092.
Miller, R.F., 2005. Biology, ecology, and management of western juniper (Juniperus occidentalis).

Miller, R.F., Rose, J.A., 1995. Historic expansion of Juniperus occidentalis (western juniper) in southeastern Oregon. The Great Basin Naturalist, 37-45.
Næsset, E., 2002. Determination of mean tree height of forest stands by digital photogrammetry. Scandinavian Journal of Forest Research 17, 446-459.
Nielsen, E., Noone, M., Kagan, J.S., 2013. Western Juniper (Juniperus occidentalis) and invasive annual grass mapping in Eastern Oregon.
Nielsen, E., Poznanovic, A., Popper, K., 2014. Accuracy comparison of tree mapping methods in eastern Oregon. In. Report.
O'Callaghan, J.F., Mark, D.M., 1984. The extraction of drainage networks from digital elevation data. Computer vision, graphics, and image processing 28, 323-344.
Poznanovic, A.J., Falkowski, M.J., Maclean, A.L., Smith, A., Evans, J.S., 2014. An accuracy assessment of tree detection algorithms in juniper woodlands. Photogrammetric Engineering & Remote Sensing 80, 627-637.
Ren, S., He, K., Girshick, R., Sun, J., 2015. Faster R-CNN: Towards Real-Time Object Detection with Region Proposal Networks. In, ArXiv e-prints.
Ronneberger, O., Fischer, P., Brox, T., 2015. U-net: Convolutional networks for biomedical image segmentation. In, International Conference on Medical image computing and computer-assisted intervention. Springer, pp. 234-241.
Safdarinezhad, A., Mokhtarzade, M., Zoej, M.J.V., 2017. Coregistration of Satellite Images and Airborne LiDAR Data Through the Automatic Bias Reduction of RPCs. IEEE Journal of Selected Topics in Applied Earth Observations and Remote Sensing 10, 749-762.
Sessions, J., 2018. In.
Skurikhin, A.N., Garrity, S.R., McDowell, N.G., Cai, D.M., 2013. Automated tree crown detection and size estimation using multi-scale analysis of high-resolution satellite imagery. Remote sensing letters 4, 465-474.
Soil Survey Staff, 1999. Soil Taxonomy: A Basic System of Soil Classification for Making and Interpreting Soil Surveys. In. USDA Natural Resources Conservation Service, Washington DC, p. 886.
St. John, R., Tóth, S., 2013. Spatially explicit forest harvest scheduling with difference equations. Annals of Operations Research, 1-23.
Strand, E.K., Smith, A.M., Bunting, S.C., Vierling, L.A., Hann, D.B., Gessler, P.E., 2006. Wavelet estimation of plant spatial patterns in multitemporal aerial photography. International Journal of Remote Sensing 27, 2049-2054.
Strimbu, B.M., Paun, M., 2012. Sensitivity of forest plan value to parameters of simulated annealing. Canadian Journal of Forest Research 43, 28-38.
Strimbu, V.F., Strimbu, B.M., 2015. A graph-based segmentation algorithm for tree crown extraction using airborne LiDAR data. ISPRS Journal of Photogrammetry and Remote Sensing 104, 30-43.
Swan, L., Connolly, M., 1998. Processing and finishing western juniper. Note prepared for the Wood Technology Clinic and Show, Portland, OR.
Swan, L., Deboodt, T., Ardt, G., State of Oregon Western Juniper Legislative Report.
Tang, T., Zhou, S., Deng, Z., Zou, H., Lei, L., 2017. Vehicle detection in aerial images based on region convolutional neural networks and hard negative example mining. Sensors 17, 336.
Tzutalin, 2015. LabelImg. In.
USDA Aerial Photography Field Office, 2015. National Geospatial Data Asset (NGDA) NAIP Imagery. In. USDA Aerial Photography Field Office, Salt Lake City, Utah.
Van Deusen, P.C., 1999. Multiple solution harvest scheduling. Silva Fennica 33, 207-216.

Wang, L., Gong, P., Biging, G.S., 2004. Individual tree-crown delineation and treetop detection in high-spatial-resolution aerial imagery. Photogrammetric Engineering & Remote Sensing 70, 351-357.
Wegner, J.D., Branson, S., Hall, D., Schindler, K., Perona, P., 2016. Cataloging public objects using aerial and street-level images-urban trees. In, Proceedings of the IEEE Conference on Computer Vision and Pattern Recognition, pp. 6014-6023.
Zhen, Z., Quackenbush, L.J., Zhang, L., 2016. Trends in automatic individual tree crown detection and delineation—evolution of lidar data. Remote Sensing 8, 333.
Zhu, J.-Y., Park, T., Isola, P., Efros, A.A., 2017. Unpaired image-to-image translation using cycle-consistent adversarial networks. arXiv preprint arXiv:1703.10593.